LEIDSE GEOLOGISCHE MEDEDELINGEN, Deel 51, Aflevering 1, pp. 1–36, 1–9–1976

PETROFABRICS, MICROTEXTURES AND DISLOCATION SUBSTRUCTURES OF OLIVINE IN A PERIDOTITE MYLONITE (ALPE ARAMI, SWITZERLAND)

BY

J. M. A. BUISKOOL TOXOPEUS

ABSTRACT

The development of preferred crystallographic orientation and dimensional fabric of olivine in relation to deformation were investigated in a thin, continuous chlorite peridotite mylonite rim around the garnet peridotite body of Alpe Arami, Ticino, Switzerland. The mylonite is a foliated rock containing strained relict crystals (porphyroclasts) embedded in abundant, recrystallized matrix material. Petrofabric analysis of the porphyroclasts showed a preferred orientation (the γ_{ol} fabric) of $\gamma_{ol} = [100]$ perpendicular to the foliation plane, while $a_{ol} = [010]$ together with $\beta_{ol} = [001]$ were situated in the foliation. The matrix developed a completely different pattern (the a_{ol} fabric) of $a_{ol} = [010]$ perpendicular to the foliation, and $\beta_{ol} = [001]$ together with $\gamma_{ol} = [100]$ in the foliation. Petrofabric analysis of a wide range of specimens, however, suggested a transitional relation between these two preferred orientation patterns of the porphyroclasts and the matrix. The γ_{ol} fabric is thought to represent a rotationally unstable orientation under deformation conditions present in the mylonite, on the basis of the observed glide systems {0kl} [100]. The γ_{ol} fabric, inherited from a neighbouring chlorite peridotite, still exists because it was preserved from recrystallization by this unfavourable position for deformation. In general, however, the clasts' crystal axes have rotated towards the a_{ol} fabric orientation as observed in the many girdle fabrics. During this process, recrystallization took place at the rims of the clasts establishing the a_{ol} fabric in the matrix. A sequence of microtextures, depending on the strain conditions in the mylonite, have been observed, showing this gradual transition. Matrix grains situated in strain protected areas to the side of porphyroclasts, still showed an inherited γ_{ol} fabric because in these areas rotations towards a new deformation position were small. Thin matrix grains in high strain regimes showed the a_{ol} fabric, a rotationally stable deformation orientation they could not change. Just recrystallized porphyroclasts, present in the matrix as spherical agglomerates just fully exposed to the strain, occupy positions concerning habit and location between the grains in high strain regimes and the porphyroclasts, exhibiting transitional fabrics.

Crystal plasticity is an important mechanism allowing deformation and development of the observed preferred orientations. High voltage electron microscopy was used to determine glide systems and dislocation substructures in the porphyroclasts and in the matrix. The porphyroclasts showed evidences for strong polygonization during dynamic recovery, while in the matrix a continuous process of dynamic recrystallization proceeded concurrently with deformation after some critical strain, in the form of nucleation and grain growth. In this cyclical process in the matrix, the dynamic recovery was still present, giving rise to some anology with the dislocation substructures in the porphyroclasts. The electron microscope observations allowed an adequate explanation for the transition from γ_{ol} to a_{ol} fabrics.

CONTENTS

Part II

PART I

CHAPTER I

INTRODUCTION

INTRODUCTORY REMARKS

Olivine, the main constituent of peridotite, is the subject of profound interest because the possible upper mantle origin of the material can be used for a basic understanding of the deformation processes and conditions in this part of the mantle.

Much recent research in peridotites is focussed on the problem of development of preferred crystallographic orientation and dimensional fabric in relation to deformation.

The aim of this paper is to study the fabric development in a mylonite in connection with the natural deformation and recrystallization processes.

Petrofabric analysis (including axial distribution analysis) and high voltage electron microscopy are used to study olivine in a thin, continuous chlorite peridotite mylonite rim around the garnet peridotite body of Alpe Arami, Ticino, Switzerland (Fig. 1).

This mylonite is a foliated rock, containing strained relict crystals (porphyroclasts) embedded in abundant recrystallized matrix material (see Bell & Etheridge, 1973). There are two distinct types of preferred crystallographic orientation in the mylonite, connected with the porphyroclasts and the matrix respectively. These different preferred orientations of olivine form the basis of further investigation.

The porphyroclasts usually show a $\gamma = [100]$ olivine pointmaximum perpendicular to a foliation plane, while the matrix grains show an $\alpha = [010]$ olivine pointmaximum perpendicular to the same foliation plane (Fig. 4).

The main problem is to explain these two different preferred orientations as tectonic fabrics, probably connected with different conditions of deformation during the generation of the mylonite.

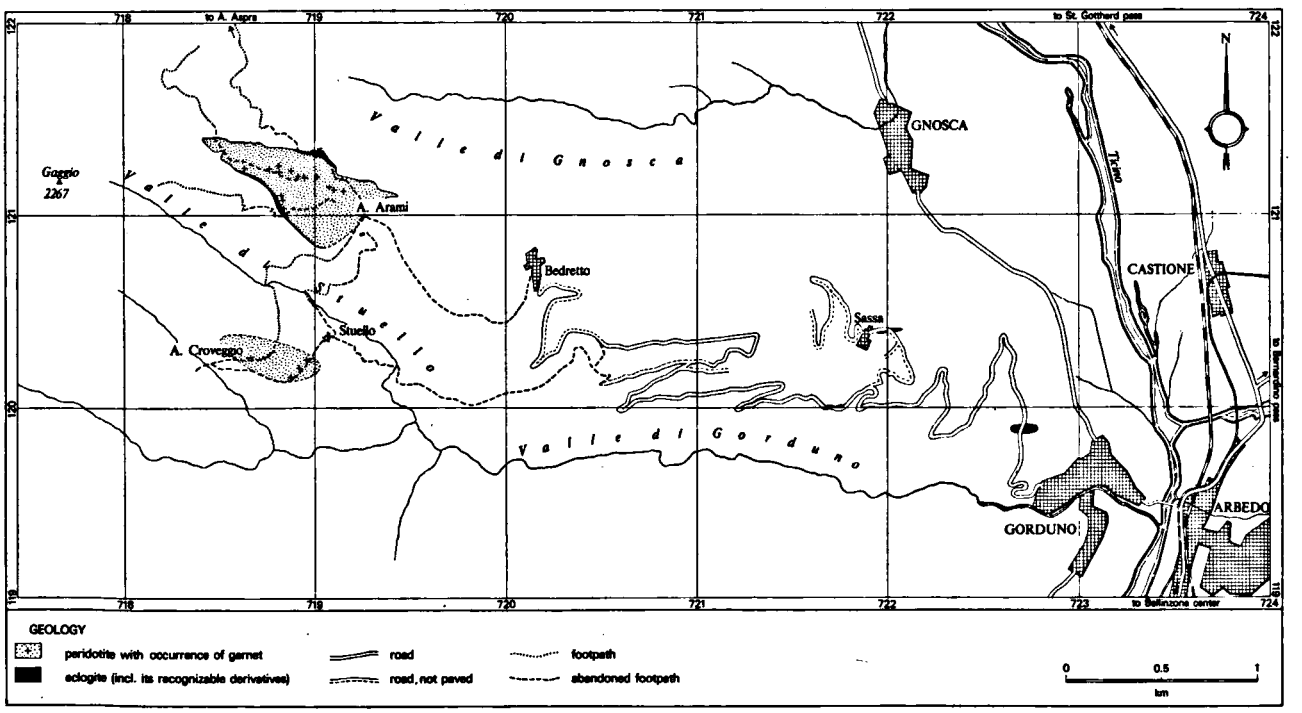

Fig. 1. Simplified map of the situation of Alpe Arami (after Möckel, 1969).

The $\gamma = [100]$ fabric in the porphyroclasts is an extremely rare fabric in olivine, and apart from Alpe Arami (Möckel, 1969) it has been reported only from three other peridotites (Yoshino, 1961 & 1964; Kazakov, 1965; Littlejohn & Greenwood, 1974).

Petrofabric analysis suggests a transitional relation between the crystallographic orientation patterns of the porphyroclasts and the matrix grains (Part I, Chapter II). Axial distribution analysis (AVA) reveals the relation between positions of individual grains and their crystallographic orientation (Part I, Chapter III). A sequence of microstructures is examined using this technique, and a correlation of fabric with microstructures allows a postulate to be made for the evolution of the fabric in the mylonite matrix. Significantly, in this paper, high voltage electron microscopy techniques have been used to study in detail the deformation and recrystallization features in the olivine porphyroclasts and matrix grains (Part II).

Crystal plasticity in olivine is suggested as an important mechanism allowing deformation and development of the observed preferred crystallographic orientation patterns. The slip systems and dislocation substructures observed in the porphyroclasts and the matrix grains, make it difficult to explain the $\gamma = [100]$ olivine fabric as produced during deformation. These observations allow, however, an adequate explanation of the transition from $\gamma = [100]$ to $\alpha = [010]$ fabrics observed in the mylonite rim.

GENERAL GEOLOGY OF THE GARNET PERIDOTITE

The garnet peridotite occurrence of Alpe Arami near Bellinzona, in the Swiss Canton Ticino, was investigated for its structural petrology by Möckel (1969); see also Grubenmann (1908); Dal Vesco (1953); O'Hara & Mercy (1966); Rost et al. (1974).

The following history is a summary of Möckels work (Table 1). In Alpe Arami, evidence is available of three main tectonic phases (F'_0, F''_0, F_1), associated with three metamorphic facies (eclogite, granulite and amphibolite facies). The garnet peridotite, originally during eclogite facies metamorphism, developed a layering (S_L) with a preferred orientation of $\gamma = [100]$ olivine perpendicular to S_L, and $\alpha = [010]$ olivine together with $\beta = [001]$ olivine parallel to S_L in girdle distributions. In the retrograde granulite facies, S_L was folded by F_0'', giving rise to a foliation S_0 as the axial fold plane in a spinel-amphibole peridotite. According to Möckel (1969), the $\gamma = [100]$ olivine orientation changes from perpendicular to S_L, to the new orientation $\gamma = [100]$ olivine perpendicular to S_0. This feature suggests a tectonic origin for the $\gamma = [100]$ olivine preferred orientations perpendicular to the foliation.

The last tectonic phase of importance, the alpine main phase F_1, developed an S_1 cleavage in the peridotite body. The S_1 cleavage plane is developed with a variable intensity in the peridotite body and may be defined by a chlorite preferred orientation of (001) parallel to S_1. According to Möckel (1969) the preferred orientations of olivine, orthopyroxene and amphibole were not affected by this phase. Together with the F_1 phase a chlorite peridotite in amphibolite facies was developed. The F_1 phase was probably also responsible for the development of the chlorite peridotite mylonite rim around the body under amphibolite facies conditions (Möckel, 1969, p. 120). Möckel (1969) suggested that the foliation plane in the mylonite is an S_1 plane on the basis of the chlorite fabric. Recent field observations (see below), however, suggest a more or less continuous mylonite rim around the peridotite body, with a foliation plane parallel to the margin of the

TECTONIC PHASE	PERIDOTITE					ECLOGITES	GNEISSES, ETC.
	peridotite type	mineral paragenesis	megascopic structures	mineral orientations	metamorphic facies		
?	?	titanclinohumite + ... ?	?	?	?	S_o	(S_3 foliation?, bedding?)
F'_0 (pre-Alpine?)	garnet-peridotite	olivine, orthopyroxene, clinopyroxene and garnet	S_o, l'_0	olivine $\gamma_{ol} \perp S_L (k=1.0)$ orthopyroxene $\beta_{opx} \perp S_L (k=2.9)$ clinopyroxene $c_{cpx} // l'_0 (k=2.7)$	eclogite facies		

F''_0	spinel-amphibole-peridotite
	spinel-amphibole-peridotite-mylonite
		olivine, orthopyroxene, amphibole and spinel (± clinopyr.)	S_o, l'_0
			S_m
				olivine $\gamma_{ol} \perp S_o (k=1.3)$
				orthopyroxene $c_{opx} // l'_0 (k=3.4)$
				amphibole $c_{amph} // l'_0 (k=2.7)$
				mylonite:
				olivine no distinct relation to megascopic structures
				orthopyroxene almost no preferred orientation
					granulite facies		

F_1 (Alpine main phase)	chlorite-peridotite chlorite-peridotite-mylonite	olivine, orthopyroxene, amphibole and chlorite	S_1, l_1	olivine, orthopyroxene, amphibole: orientation unaffected by F_1 chlorite $\pi\{001\}_{chl} \perp S_1$ mylonite: olivine (porphyroclasts) $\gamma_{ol} \perp S_1 (k=1.8)$ olivine (matrix) $\alpha_{ol} \perp S_1 (k=2.4)$ chlorite (matrix) $\pi\{001\}_{chl} \perp S_1 (k=8.2)$	amphibolite facies	S_1, l_1 amphibole	S_1, l_1 amphibole, biotite
F_2			S_2 ?				S_2, l_2 biotite
F_3							S_3, l_3
	serpentinite	serpentine, carbonate and talc	vertical, N-S striking talc veins		greenschist facies		

Table 1. Structural-petrological evolution of the peridotite of Alpe Arami and its country rocks (after Möckel, 1969).

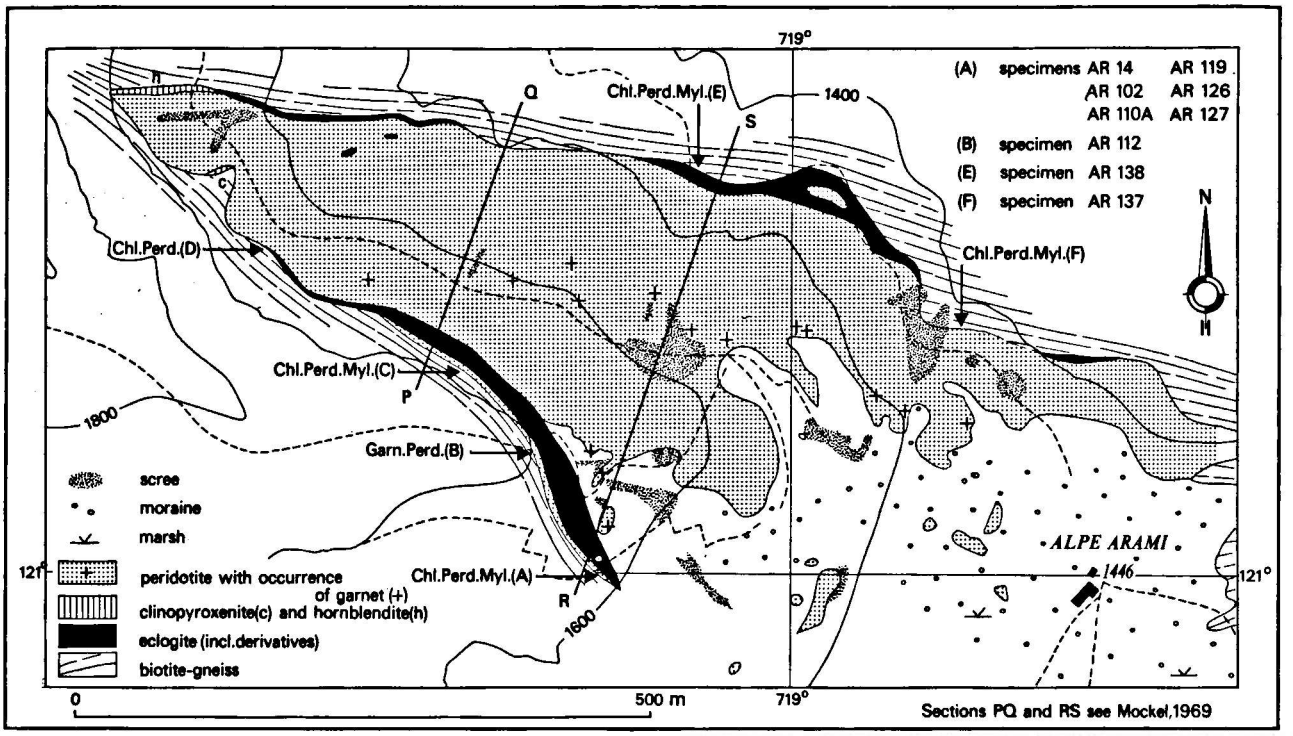

Fig. 2. Geological map of Alpe Arami (after Möckel, 1969).

body. This implies in certain areas an angular relationship between the foliation plane in the mylonite (S_{myl}), and the S_1 cleavage plane. Poor exposure did not reveal this situation clearly. In most cases, however, S_1 is parallel to the foliation plane in the mylonite.

THE CHLORITE PERIDOTITE MYLONITE

Occurrence

Field observations gave evidence for a more or less continuous mylonite rim around the entire garnet peridotite body (Fig. 2); this is additional to Möckel, who described only one occurrence (AR 14). The width of the mylonite varies from 10 cm tot 3 m and is often difficult to determine in the field. Frequently the mylonite is found interlayered with the chlorite peridotite, showing sharp contacts.

Petrography

On a microscopic scale, olivine porphyroclasts (⌀0.5–3 mm) and matrix material (⌀0.1 mm) can be distinguished.

About 15% of the observed porphyroclasts are orthopyroxene or amphibole. The matrix consists of about 80% of olivine with inhomogeneously distributed variable quantities of orthopyroxene, amphibole and chlorite.

The olivine is anhedral with a distinct (010) cleavage and sometimes a (100) cleavage. The optic angle, $2V = 88°$, ($r < v$ weak), corresponds to a composition of $Fo_{91}Fa_9$

Fig. 3. The chlorite peridotite mylonite, strained olivine porphyroclasts embedded in recrystallized matrix grains.

(O'Hara & Mercy, 1963; Mercy & O'Hara, 1965). Rutile needles and fluid(?) inclusions are observed in the olivine (Möckel, 1969).

Olivine porphyroclasts usually possess undulatory extinction and kink boundaries parallel to (100). 30% of the grains exhibit sharp extinction; so it can be concluded that most of the porphyroclasts show optical evidence for defects in their crystal lattice (see Part II). Their external shape is always rounded and commonly flattened in the foliation plane (S_{myl}) (Fig. 3), occasionally showing evidence of external rotation. The grain boundaries of the porphyroclasts are curved and generally scalloped.

The olivine matrix crystals define a polygonal aggregate with straight to slightly curved grain boundaries and many triple point junctions (Ragan, 1969). The matrix grains are equidimensional or flattened in the foliation plane (S_{myl}). These various external shapes of the crystals define specific microtextures (Chapter III) in different regions of the rock.

Serpentine (α-chrysotile) is present along almost all the grain boundaries in the mylonite, and in cracks in the porphyroclasts (Fig. 45). Together with the serpentine an abundance of chlorite (negative elongation, (001) twinning) is present. The chlorite, a retrograde product of garnet, is generally found smeared out through the whole rock, thus helping to define the foliation plane. The chlorite possesses a strong preferred orientation of $\pi(001)$ perpendicular to the foliation plane (S_{myl}), (Möckel, 1969, p. 118/119), Fig. 4. Although the chlorite is generally diffused through the whole rock defining the foliation plane, chlorite aggregates are present in some regions. These strongly flat-

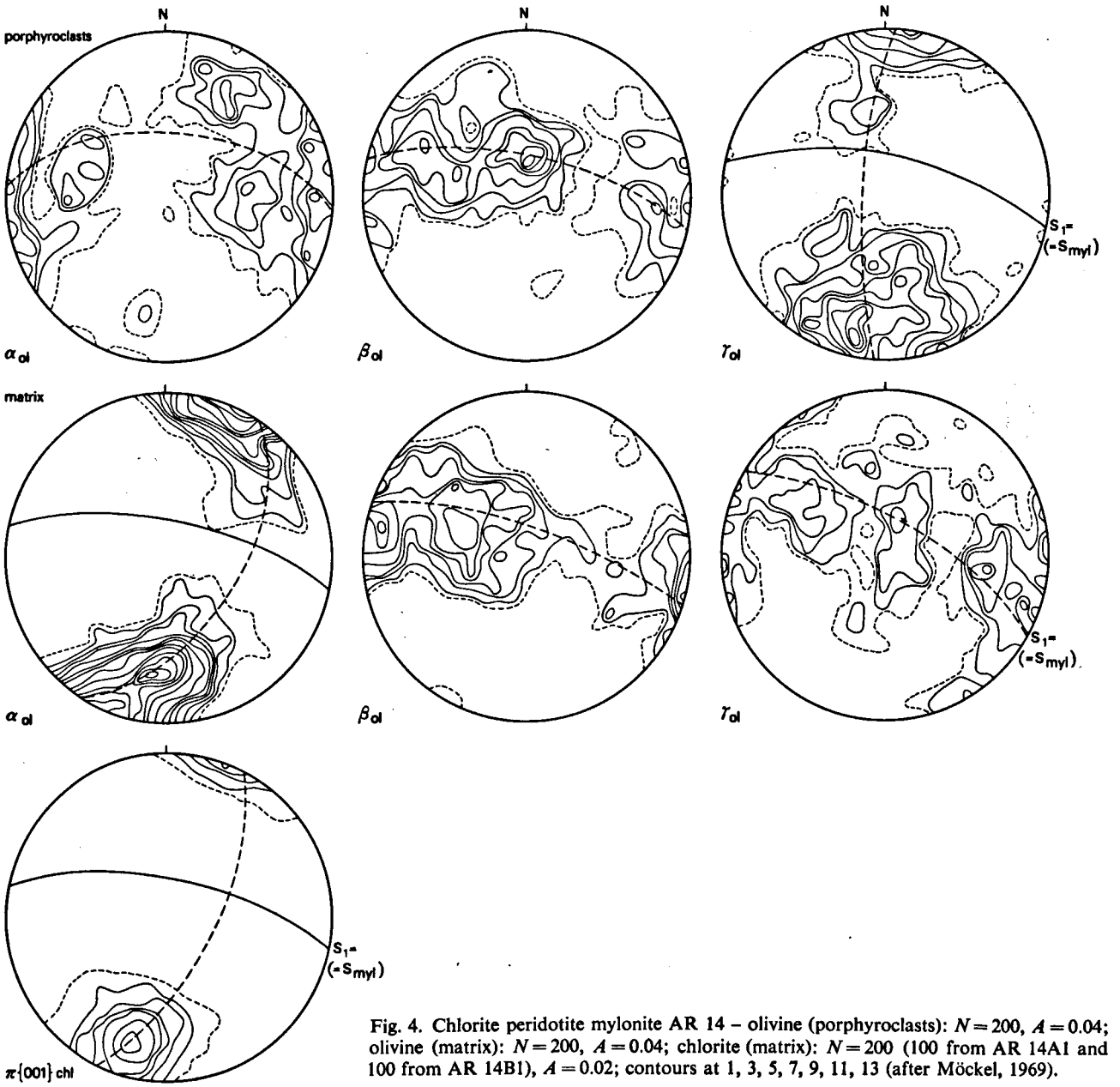

Fig. 4. Chlorite peridotite mylonite AR 14 – olivine (porphyroclasts): $N=200$, $A=0.04$; olivine (matrix): $N=200$, $A=0.04$; chlorite (matrix): $N=200$ (100 from AR 14A1 and 100 from AR 14B1), $A=0.02$; contours at 1, 3, 5, 7, 9, 11, 13 (after Möckel, 1969).

tened knobs are believed to represent external forms of primary garnet, or secondary spinel-amphibole aggregates converted to chlorite.

The most prominent mesoscopic microstructure in the mylonite is a grain shape foliation (S_{myl}) defined by flattened olivine grains and a mineralogical layering of chlorite. The S_{myl} has developed local curvatures around porphyroclasts or just recrystallized porphyroclasts. On the mesoscopic scale, S_{myl} appears to be a continuous plane parallel to the rim of the peridotite body.

In the mylonite no mesoscopic lineation is observed.

Storage. – The location of the samples mentioned in the text is indicated on the map (Fig. 2). The samples are numbered from RGM 249773 up to and including RGM 249801, and are stored at the Rijksmuseum van Geologie en Mineralogie in Leiden, The Netherlands.

CHAPTER II

PETROFABRIC ANALYSIS

INTRODUCTION

The optical directions α, β and γ of olivine have been measured with a five-axis stage (Emmons, 1943), using methods developed by Möckel (1969). In correspondence with the orthorhombic symmetry of olivine the following nomenclature is used: $\alpha = [010]$, $\beta = [001]$, $\gamma = [100]$ (after Deer, Howie & Zussman, 1962).

The fabric diagrams were constructed on the IBM 370/158 computer at the Computer Centre of Leiden University, with the aid of Fortran IV programs, developed by Möckel (1969 & 1970). Separate diagrams for α, β and γ have been plotted on the lower hemisphere, equal area projection. All diagrams are projections with the S_{myl} oriented vertically.

In the explanatory text, N is the number of grains measured, A is the area of the counting circle compared with the area of the hemisphere (= 1). The size of the area of the counting circle is chosen depending on the number of measurements (N). In general a sample size of $N = 100$–200, with $A = 0.02$, is used for the construction of the diagrams. The computer output of the diagrams shows lower hemisphere projections with frequency[1]) distributions at counting points.

Density contours were drawn between the counting points, to indicate areas with equal frequencies. Density 1 is always shown as a dashed line, while density 5 is represented by a bold contour.

SAMPLING PROCEDURES

The following techniques were used to obtain representative samples of the distributions of olivine grain orientations. First, small samples were obtained either by:

A. random sampling of 100 grains, or

B. sampling from photographs of a thin section; all the grains within a strip drawn perpendicular to an S-plane were measured.

These two methods were repeated several times in one section.

[1]) Frequency of a class is the number of measurements in that class; frequency density within a class is found by dividing the relative frequency by the width of the class; relative frequency of a class is equal to its frequency divided by the total number of measurements such that the sum of the relative frequencies equals 1. $d = n/N.A$ = frequency density; n = frequency = number of measurements within the counting circle.

A representative population was reached when combined samples of the orientation distribution gave the same pattern elements.

Thin sections of three mutually perpendicular orientations in each handspecimen were used (one parallel to S_{myl}, two normal to S_{myl}).

All results have been checked to be reproducible.

THE PORPHYROCLASTS

TYPE 1 (= the *T*-fabric)	TYPE 2	TYPE 3+4
AR 1481	AR 14A1	AR 110A AR 102
mentioned in text		
other samples		
AR 1482	AR 119 AR 126 AR 112A	AR 127 AR 138

THE MATRIX

TYPE A (= the α-fabric)	TYPE B
AR 1481 AR 137C	AR 14A1 AR 110A AR 102
mentioned in text	
other samples	
AR 138 AR 126	AR 127 AR 119 AR 112A AR 1482

Table 2. Distribution of fabric types in studied samples in the mylonite.

ORIENTATIONS OF OLIVINE IN THE MYLONITE

The following types of preferred orientation patterns can be distinguished:

A. *The porphyroclasts* (Table 2)

The orientation patterns for olivine porphyroclasts can be classified in three main groups:

Type 1 (the γ_{ol} fabric). – This fabric is the group mentioned by Möckel as forming the characteristic mylonite fabric (Möckel, 1969, p. 119). A more refined analysis reveals the following patterns (Fig. 5):

1. α_{ol} generally weak preferred orientation forming a girdle pattern perpendicular to S_{myl} with submaxima close to S_{myl};
2. β_{ol} pointmaxima in girdle pattern parallel to S_{myl};
3. γ_{ol} strong preferred orientation in a pointmaximum close to πS_{myl}.

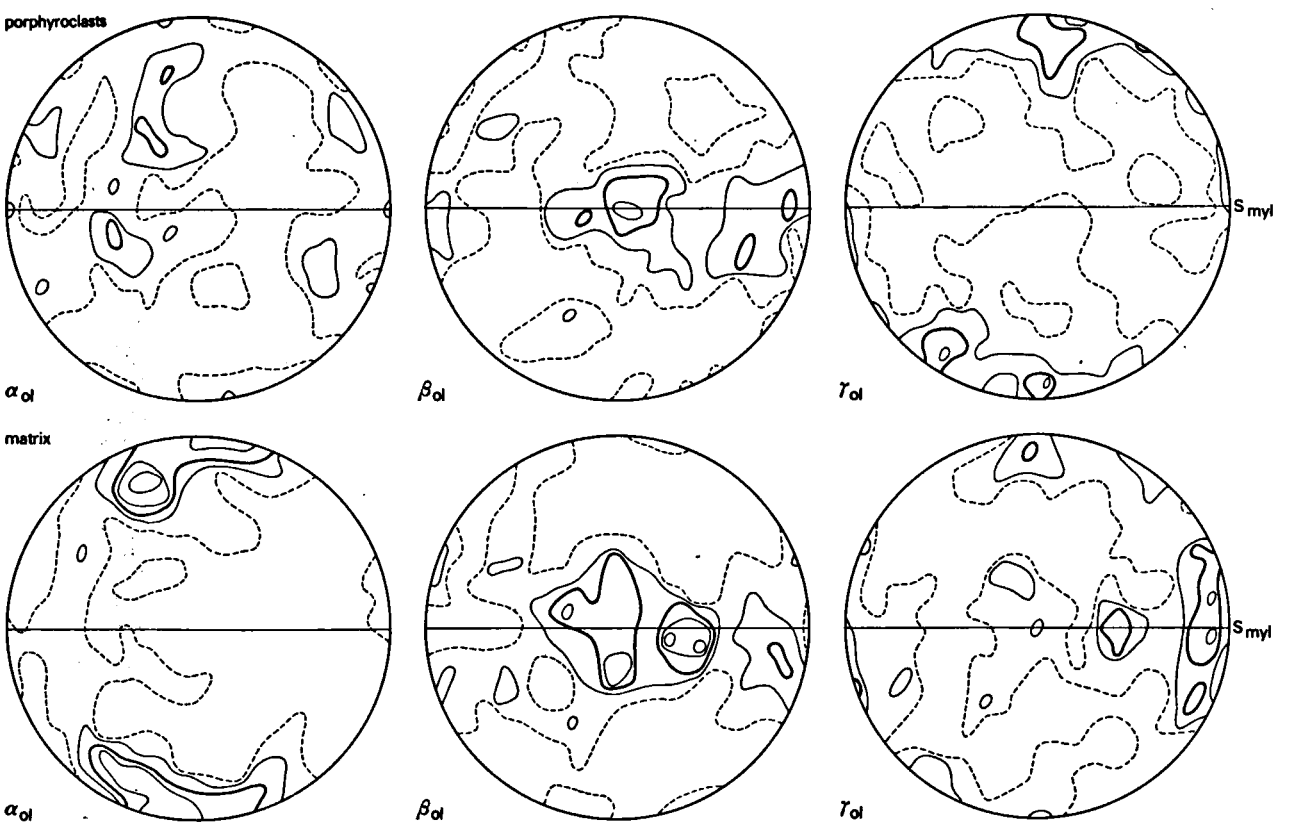

Fig. 5. Chlorite peridotite mylonite AR 14B1 – olivine porphyroclasts (fabric type 1): $N = 100$, $A = 0.02$; olivine matrix (fabric type A): $N = 100$, $A = 0.02$; contours at 1, 3, 5, 7, 9.

In the same handspecimen (AR 14), however, the γ_{ol} fabric grades into:

Type 2 (Fig. 6). –
1. α_{ol} orientations defining a girdle pattern at high angles to S_{myl} with submaxima along the girdle;
2. β_{ol} pointmaxima in girdle pattern parallel to S_{myl};
3. γ_{ol} pointmaxima showing a tendency to rotate towards S_{myl}.

In other handspecimens of the same exposure, a third group, containing types 3 and 4, can be distinguished:

Types 3 and 4 (Figs. 7, 8). –
1. α_{ol} shows random orientations, perhaps with some preference for S_{myl}, and a great circle distribution perpendicular to S_{myl};
2. β_{ol} weak preferred orientations, always parallel to S_{myl};
3. γ_{ol} forming great circle distributions with submaxima close to πS_{myl} and S_{myl}.

Slight differences between types 3 and 4 can be noticed in the distribution of γ_{ol} (type 3: girdle pattern normal to S_{myl}; type 4: pointmaximum close to πS_{myl} arranged in a weak girdle pattern normal to S_{myl}).

B. *The matrix material* (Table 2)
In general the orientation of the olivine matrix grains does not show much difference in the three groups of fabrics mentioned above.

General features of the main fabric (the α_{ol} fabric) are (Table 2, type A):
1. α_{ol} pointmaxima perpendicular to S_{myl};
2. β_{ol} elongated pointmaximum to girdle fabric parallel to S_{myl};
3. γ_{ol} elongated pointmaximum to girdle fabric with submaxima parallel to S_{myl}.

These main features can be supplemented with trends to produce complicated fabrics with the following properties (Table 2, type B):
1. α_{ol} may produce a girdle fabric perpendicular to S_{myl}, and so approach S_{myl};
2. β_{ol} may produce a girdle fabric parallel to S_{myl};
3. γ_{ol} may produce orientations close to πS_{myl}.

C. *Description of the studied samples*

The following specimens were selected as representative samples for the above-mentioned types of preferred orientations (Table 2):

1. *Specimen AR 14B1* (Fig. 5). – See also Möckel (1969). The olivine porphyroclasts show their strongest preferred orientation in a pointmaximum of γ_{ol} close to the pole of S_{myl} (πS_{myl}). β_{ol} is concentrated in a girdle pattern with strong submaxima along S_{myl}. The preferred orientation of α_{ol} is weakly parallel

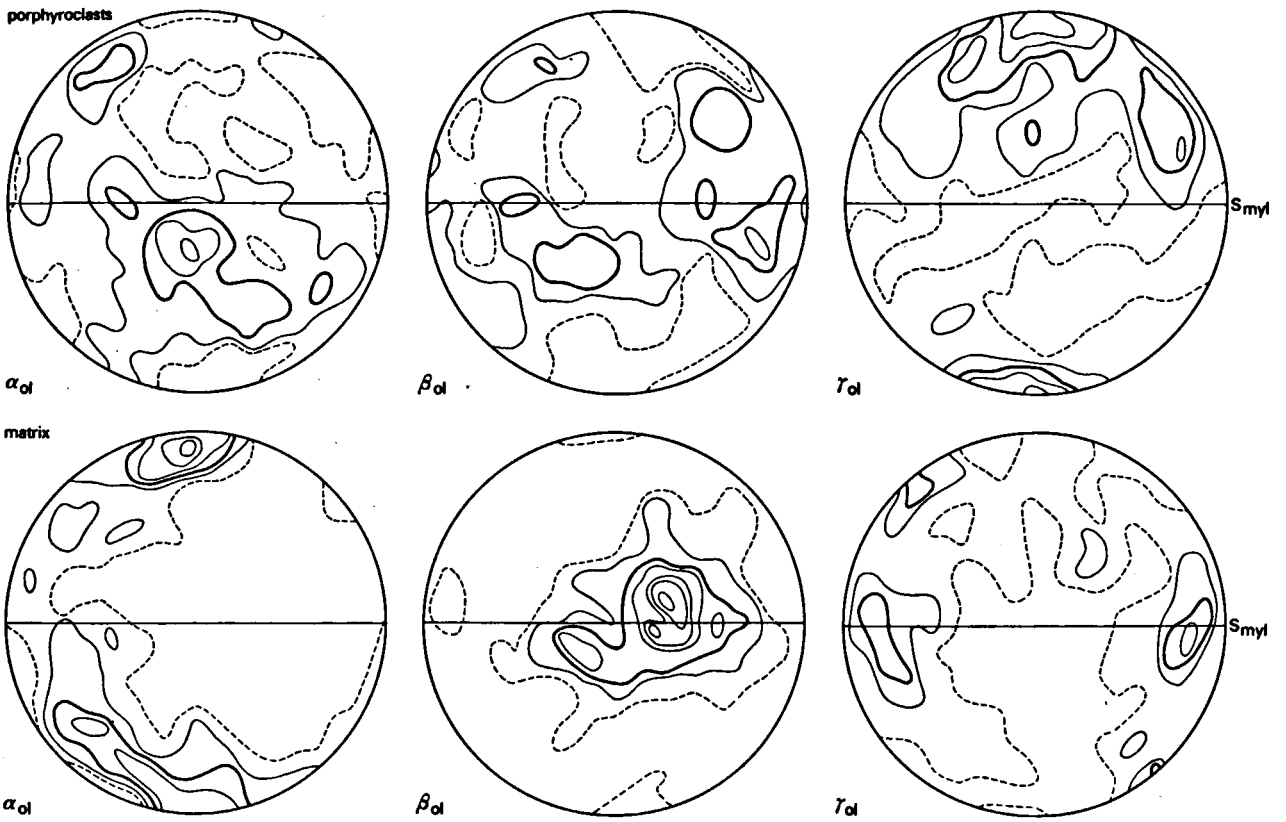

Fig. 6. Chlorite peridotite mylonite AR 14A1 – olivine porphyroclasts (fabric type 2): $N = 75$, $A = 0.04$; olivine matrix (fabric type B): $N = 100$, $A = 0.02$; contours at 1, 3, 5, 7, 9, 11, 13.

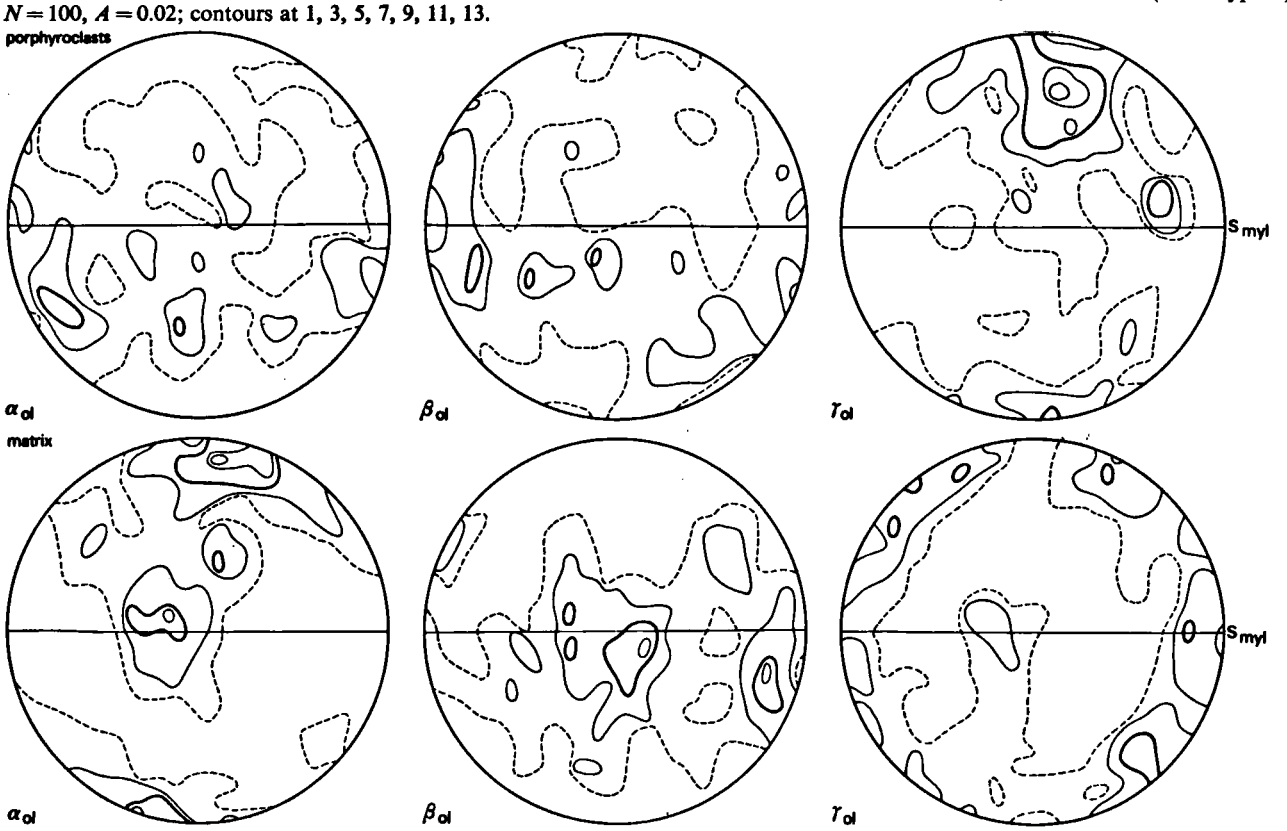

Fig. 7. Chlorite peridotite mylonite AR 110A – olivine porphyroclasts (fabric type 3): $N = 100$, $A = 0.02$; olivine matrix (fabric type B): $N = 100$, $A = 0.02$; contours at 1, 3, 5, 7, 9.

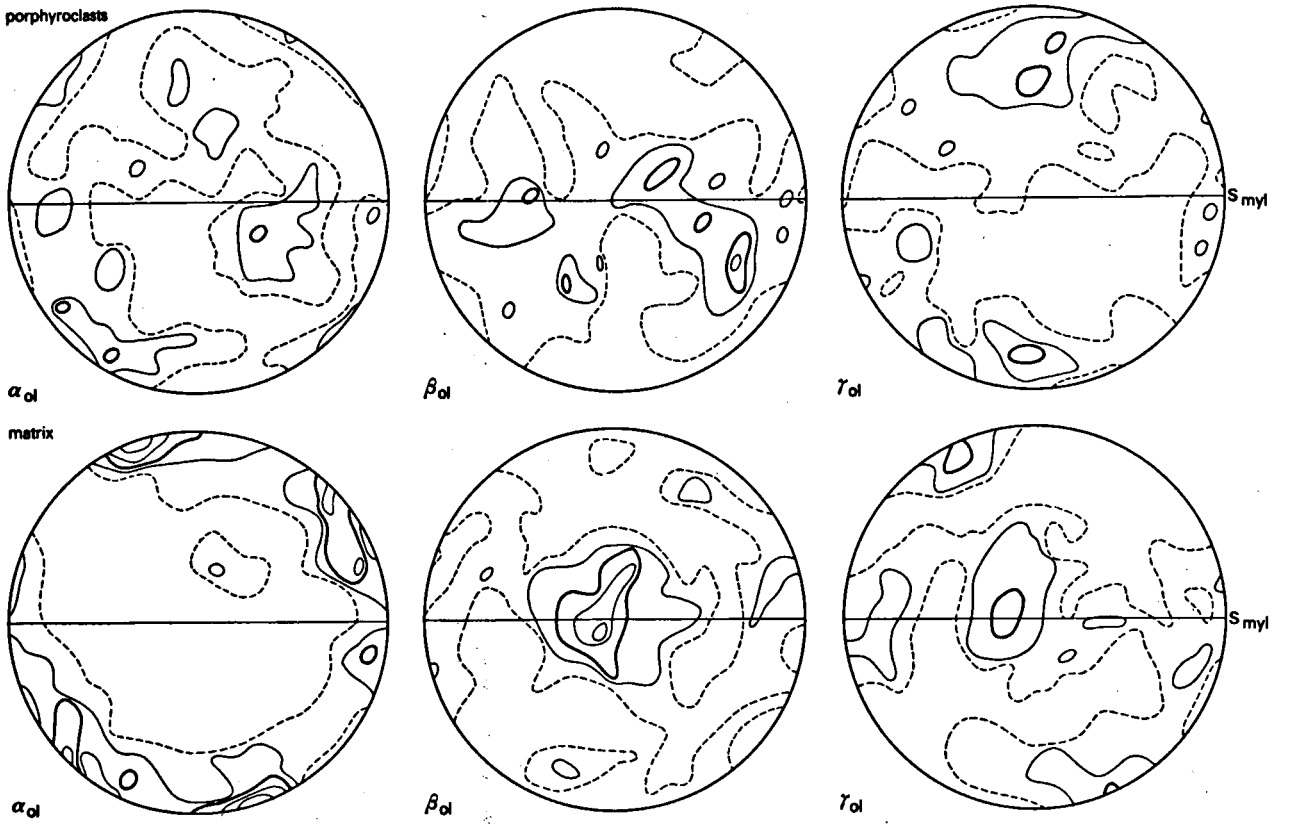

Fig. 8. Chlorite peridotite mylonite AR 102 – olivine porphyroclasts (fabric type 4): $N = 100$, $A = 0.02$; olivine matrix (fabric type B): $N = 100$, $A = 0.02$; contours at 1, 3, 5, 7, 9.

to S_{myl}, but also has a tendency to spread in a great circle perpendicular to S_{myl}. The latter great circle orientation pattern of α_{ol} in the porphyroclasts is also found in the matrix, however, with a strong broad pointmaximum of α_{ol} parallel to πS_{myl}. In the matrix, β_{ol} shows an elongated pointmaximum distribution following a great circle parallel to S_{myl}. Here γ_{ol} shows weak preferred orientation patterns with a tendency to spread into S_{myl}, but orientations close to πS_{myl} do also occur.

2. *Specimen AR 14A1* (Fig. 6). – See also Möckel (1969). The overall orientations do not deviate much from AR 14B1, with the exception of a more pronounced development of α_{ol} and γ_{ol} girdle patterns normal to S_{myl}, a tendency already noticeable in AR 14B1. In the porphyroclasts, α_{ol} is arranged in a great circle inclined at a large angle (about 70°) to S_{myl} with a submaximum near S_{myl}, while β_{ol} follows a great circle along S_{myl}. The orientation of γ_{ol}, an elongated pointmaximum normal to S_{myl}, shows an approach towards S_{myl} in a great circle normal to S_{myl}. A great circle distribution perpendicular to S_{myl} with an elongated maximum close to πS_{myl} is the orientation of α_{ol} in the matrix. Here β_{ol} shows an elongated pointmaximum in S_{myl}, while γ_{ol} is weakly oriented along a great circle perpendicular to S_{myl}, with preferences for positions close to S_{myl}, but other orientations also occur.

3. *Specimen AR 110A* (Fig. 7). – The orientations of α_{ol} and β_{ol} of the porphyroclasts show weak preferred directions. α_{ol} is randomly oriented within one half of the projection, while β_{ol} shows preferred orientations along S_{myl}. γ_{ol}, in great circle distribution perpendicular to S_{myl}, shows a pointmaximum close to πS_{myl}, and a submaximum near S_{myl}. In the matrix, α_{ol} is oriented in a great circle distribution normal to S_{myl}, with a pointmaximum nearly perpendicular to S_{myl}, and a submaximum in S_{myl}. Here β_{ol} is arranged in a girdle pattern with submaxima parallel to S_{myl}, while γ_{ol} is oriented in submaxima within a girdle pattern normal to S_{myl}.

4. *Specimen AR 102* (Fig. 8). – The α_{ol} orientation of the porphyroclasts is at random; β_{ol} possesses a great circle distribution with submaxima parallel to S_{myl}, and γ_{ol} is oriented close to πS_{myl}, but orientations near S_{myl} also occur. In the matrix, α_{ol} is oriented in submaxima within a girdle pattern normal to S_{myl}, with preferred orientations close to πS_{myl} and S_{myl}; β_{ol} is oriented in a pointmaximum in S_{myl}, and γ_{ol} is distributed in submaxima parallel to S_{myl}, and near πS_{myl}.

DISCUSSION

The main result arising from the analysis of the preferred orientation patterns suggests a transition from fabrics with γ_{ol} perpendicular to S_{myl} (porphyroclasts) into fabrics with α_{ol} perpendicular to S_{myl} (matrix).

It is postulated that this transition from the γ_{ol} to the α_{ol} fabric is caused by plastic deformation under conditions relevant to the formation of the mylonite rim.

From electron microscopy on naturally (Part II) and experimentally deformed olivines, and from optical microscope analysis (see Avé Lallemant & Carter, 1970; Buiskool Toxopeus & Boland, 1976; Carter, 1971; Carter & Avé Lallemant, 1970; Carter, Baker & George, 1972; Carter, Raleigh & Decarli, 1968; Green, 1974; Green &

Radcliffe, 1972a, 1972b, 1972c; Klosterman & Buseck, 1973; Raleigh, 1968; Raleigh & Kirby, 1970; Young, 1969) it has been established that prismatic glide on {0kl} [100] is the main slip system present in both the porphyroclasts and the matrix grains. Another, perhaps less important slip direction parallel to $\beta = [001]$, is represented by mainly individual screw dislocations with Burgers vector $\mathbf{b} = [001]$ (cf. Part II). Analysis of Burgers vectors show that dislocations with $\mathbf{b} = [001]$ are mainly found in the matrix, although, even in this material $\mathbf{b} = [100]$ dislocations predominate.

Before interpreting the preferred orientations and the origin of the fabrics, the major problem of the mode of deformation during the generation of the mylonite should be discussed.

Deformation models

Three essentially different models are selected to approach the deformation process. These models are used to predict the preferred orientation patterns on the basis of idealized, but actually observed glide systems.

A. *The pure shear or flattening model, considering one glide system.* – In this model the strain is coaxial; the deformation is non-rotational. During the deformation, the active slip system causes rotation of the crystal axes of the grains towards the orientation with the glide plane normal to the shortening axis (Z), and the slip direction (Burgers vector) parallel to the extension axis (X). This is the final orientation expected when the glide system tends to rotate the crystal into the most unfavourable position for continued operation of dislocation glide.

For olivine this model implies an orientation of $\gamma_{ol} = [100]$ and $\beta_{ol} = [001]$ in the flattening plane (S_{myl}), and consequently $\alpha_{ol} = [010]$ oriented normal to the flattening plane, for operation of the (010) [100] or (010) [001] glide systems. This model corresponds with the observed α_{ol} fabric in the matrix. Its final α_{ol} fabric orientation represents the hardest deformation position of the grains.

B. *The pure shear or flattening model, considering symmetrical disposition of two glide systems.* – In the metallurgical literature concerned with fabric development in FCC metals during coaxial deformation, models such as those of Calnan and Clews (1950, 1951a, b), predict that crystal axes of deformed grains rotate towards end orientations where the two or three active glide planes are symmetrically disposed towards the shortening direction (Etchecopar, 1974). It should be noted, however, that the principal stress axes are likely to be inclined to the foliation plane. The incremental axis of shortening for example may be disposed at 45° (approximately) to the shear plane. If the (100) [001] and (001) [100] systems were equally active and symmetrically disposed to the incremental shortening axis, these systems resulted in preferred orientations of either γ_{ol} or β_{ol} parallel to the shear plane, and the other direction normal to this plane. Also other possible glide systems are predicted by the model to produce such symmetrically arranged patterns.

In the present fabric study no fabrics with such symmetrical shape towards the shortening/extension axes have been recorded in the mylonite. The fabrics predicted by this model are not developed and therefore the model is rejected.

C. *The simple shear model.* – In this model there is a shear strain; the deformation is rotational. The glide systems tend to rotate the crystals into a position in which the glide plane is parallel to the shear plane (Etchecopar, 1974). In general the extension (foliation plane) is not parallel to the shear plane; however, in regimes in which a large shear was operative (mylonites?) this angle becomes small ($< 3°$). Therefore this model can result in orientations of the glide plane quasi parallel to the foliation plane, and glide directions quasi parallel to the extension axis, in cases of large shear. The crystals are rotated into a position which is most favourable for continued operation of the glide system.

The olivine orientations for this model are γ_{ol} and β_{ol} in the foliation plane, and α_{ol} normal to the foliation plane (the α_{ol} fabric in the matrix) for glide on (010) [100], (010) [001]. In this model the final α_{ol} fabric represents the softest possible deformation orientation of the grains.

It can be concluded from these models that the preferred orientation pattern in the matrix (the α_{ol} fabric) can be explained by two different deformation models. Petrofabric analysis can not decide in this case which model is more consistent with the deformation in the mylonite.

Although simple shear is generally accepted as a model for mylonitization (Nicolas et al., 1972 & 1973; Etchecopar, 1974), crystal shapes in the Alpe Arami mylonite are not indicative for this model. Features described by Etchecopar (1974) as typically pointing to shear ('cristeaux bloqués', 'cristeaux en cornues', and fracturing normal to the foliation plane) have not been observed in this material.

Commonly, γ_{ol} and β_{ol} orientations in the mylonite fabrics show a variable distribution from girdle patterns parallel to the flattening plane to elongated pointmaxima in the flattening plane. Although a decrease in fabric symmetry from pointmaxima to girdle fabrics is not proved to be connected with a difference in the deformation process (Paterson & Weiss, 1961), it is suggested that simple shear and flattening, respectively, were responsible for these fabrics.

A combined process of flattening with some simple shear (flow) seems to be a realistic deformation model for the mylonite. Locally, one of the two processes can dominate over the other, giving specific preferred orientation patterns.

The expected orientation from dislocation glide mechanisms {0kl} [100] and glide along [001], however, is not inconsistent with the main matrix orientation: the α_{ol} fabric (α_{ol} normal to S_{myl}, and γ_{ol} together with β_{ol} in S_{myl}).

The γ_{ol} orientation perpendicular to S_{myl} can not be explained by observations of dislocation substructures, and by the present glide systems. Therefore the cause of this γ_{ol} fabric orientation remains to be solved. It can only be shown that it represents a rotationally unstable position

that rotates during deformation into the orientation for the α_{ol} fabric.

It should be kept in mind that the observed dislocation arrangements do not supply enough systems for the von Mises condition to be fulfilled (see von Mises, 1928; Taylor, 1938). This does not allow olivine to attain general strains by dislocation glide alone (Paterson, 1969, for the consequences).

The matrix

The dislocation arrangement in the matrix is consistent with orientations of $\gamma_{ol} = [100]$ and $\beta_{ol} = [001]$ ending up in the plane of flattening (S_{myl}), and consequently $\alpha_{ol} = [010]$ normal to S_{myl}. This preferred orientation, caused by a dislocation glide mechanism, is found in the matrix in the form of the α_{ol} fabric. The recrystallized grains in the matrix possess a strong preferred orientation consisting of three pointmaxima (Chapter III, AR 137C) defining the α_{ol} fabric. This pattern of preferred orientations suggests that the matrix grains acquire a rotationally stable end orientation which they can not change by further deformation in respect of the strain axes. The main fabric of the matrix may represent such a final stage. In this case the grains were able to rotate and recrystallize into their final orientation (the α_{ol} fabric) without the influence of strain inhomogeneities or previous preferred crystallographic orientations. These last two features can cause significant deviations from the α_{ol} fabric in the matrix, and are thought to be responsible for girdle patterns of α_{ol} and γ_{ol} perpendicular to S_{myl} (Table 2, type B; Chapter III).

In general the strongest, most complete α_{ol} fabric is recorded in areas far from porphyroclasts or just recrystallized porphyroclasts (Chapter III, AR 137C). These domains represent areas of high strain in which the fabric has reached a final stage.

It is believed that the reason why most of the matrix fabrics show deviations from the pure α_{ol} fabric (girdle patterns) is the bulk sampling methods, that mixed different grain populations together. In Chapter III, sampling in more carefully defined areas will reveal the meaning of the deviating girdle patterns.

The porphyroclasts

From description of the preferred orientations in the porphyroclasts, it appears that the earlier mentioned γ_{ol} fabric (type 1) has gradual transitions to types 2, 3 and 4. All these fabrics are characterized by γ_{ol} orientations either perpendicular to S_{myl} (type 1), or in girdle patterns towards S_{myl} (types 2, 3 and 4). The γ_{ol} girdle patterns have a tendency to rotate until they are situated in S_{myl}, α_{ol} perpendicular to S_{myl}, and β_{ol} remaining in S_{myl}. This hypothetical end stage, which is not recorded in the porphyroclasts, constitutes the main fabric present in the matrix (the α_{ol} fabric).

From petrofabric analysis of the porphyroclasts the following features are observed:

1. the main and incipient orientation of the porphyroclasts is defined by the type 1 fabric with γ_{ol} perpendicular to S_{myl}, and α_{ol} in S_{myl};
2. there are all sorts of transitional fabrics, types 2, 3 and 4, in which γ_{ol} rotates in a great circle towards S_{myl}, and α_{ol} rotates towards πS_{myl};
3. in the porphyroclasts these transition fabrics have never reached the final stage, in which γ_{ol} should be concentrated in S_{myl}, and α_{ol} parallel to πS_{myl}, probably because recrystallization took place;
4. the final fabric, never reached in the porphyroclasts, is the main fabric in the matrix.

The porphyroclasts show to a certain extent the same dislocation arrangement as the matrix, but there are less cross arrays (slip planes) developed and more tilt boundaries.

Because a major slip direction in the porphyroclasts is parallel to $\gamma_{ol} = [100]$, no preferred orientations of γ_{ol} at high angles or perpendicular to the flattening plane, S_{myl}, are to be expected after deformation. The deviating fabric of the porphyroclasts, with γ_{ol} normal to S_{myl}, therefore can not be explained by a dislocation glide mechanism so far observed. The position γ_{ol} parallel to the shortening axis (Z) is undeformable according to the condition of von Mises (1928), unless by kinking or some other mechanism (Paterson, 1969).

The crystallographic fabric of the porphyroclasts requires explanation on the following issues:

A. why do the clasts persist in an almost completely recrystallized matrix, and

B. why do they have deviating preferred orientations observed.

These two features appear to be related to each other.

Recrystallization did not occur inside the porphyroclasts, because they were unfavourably oriented for deformation (γ_{ol} parallel to Z), and therefore they were harder to deform, and deformation was slower and not so intense.

The porphyroclasts rotate by dislocation glide on the system {0kl} [100], to obtain a more appropriate deformation position, in which γ_{ol} is oriented in S_{myl}. According to this argument the γ_{ol} fabric, with γ_{ol} nearly perpendicular to S_{myl}, is a rotationally unstable orientation under these deformation conditions. It appears that the crystal axes of the clasts rotate towards the α_{ol} fabric position, the main fabric of the matrix.

At the rims of the porphyroclasts, however, heterogeneous strain was taking place during the rotation. Recrystallization therefore was able to start at the rims of the clasts, proceeding inwards. For this reason the porphyroclasts do not exhibit α_{ol} fabrics, because usually they recrystallize before sufficient rotation of the crystal axes has taken place. The recrystallized grains at the rims have a clear relationship in crystallographic orientation to the porphyroclasts (see AVA, Chapter III). The nearest neighbour grains that recrystallized have similar orientations to the porphyroclasts. This relationship is called host control.

The reason the porphyroclasts define a γ_{ol} fabric is doubtful. Possible explanations are (i) that it could be a preservation of the primary fabric of the neighbouring (garnet-) chlorite peridotite (Möckel, 1969), or (ii) a biased or non-random selection from a completely random fabric. Because the mylonite is often interlayered with a chlorite peridotite, exhibiting a γ_{ol} fabric (Möckel, 1969), the most

favoured explanation for the γ_{ol} fabric in the mylonite is an inherited fabric. Such inheritance does not necessarily imply a random selection of grains from the preceding fabric for preservation. A non-random selection from the γ_{ol} fabric in the chlorite perioditite during deformation is more likely, selecting only the clasts defining the strongest γ_{ol} fabric, because they were harder to deform. The other explanation of type 1 fabric as a preservation of a random fabric is not likely because:

A. random fabrics do not appear to be present in the Alpe Arami peridotites;

B. the presence of specific girdle patterns (types 2, 3 and 4) is difficult to explain either as transitions from type 1, or as a preservation of a random pattern.

CONCLUSIONS

1. The porphyroclasts show a preferred orientation: the γ_{ol} fabric. This is a metastable orientation inherited on a non-representative basis from the parent or host rock. The porphyroclasts persist in this position because they are stronger and therefore harder to deform.
2. The matrix in areas of homogeneously distributed high strain possesses preferred orientation: the α_{ol} fabric.
3. The deformation process responsible for the α_{ol} fabric is consistent with two models: flattening considering one glide system, and simple shear. Dislocation glide tends to rotate the crystal into either the most unfavourable position for continued operation in the case of coaxial strain (flattening), or into the most favourable position for continued operation in the case of simple shear.
4. The distribution in the α_{ol} fabric of γ_{ol} and β_{ol} parallel to the foliation plane (S_{myl}), ranging from girdle patterns to pointmaxima, suggests that perhaps with variable intensity, both pure shear and simple shear processes were operative during the generation of the mylonite.

CHAPTER III

AXIAL DISTRIBUTION ANALYSIS (AVA)

INTRODUCTION

Although the alpha fabric (α_{ol} normal to S_{myl}) is the most common fabric in the matrix (Chapter II), girdle distributions of α_{ol} are still present. It is assumed that these girdle distributions are the result of the random sampling methods used, and that different grain orientation populations were mixed together. Therefore the overall picture of the petrofabric analysis diagrams with girdle distributions has been refined, and the pertinent procedure is outlined in this chapter. The relation between the preferred orientations of the crystals and their locations was studied with the aid of axial distribution analysis (cf. Collée, 1962), in order to distinguish between different populations.

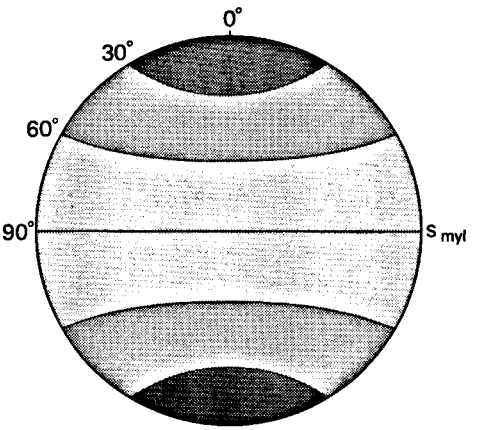

Fig. 9. Key shading AVA.

METHOD OF PREPARATION OF AN AVA

An area of interest is selected in thin section, and photographs of this area prepared. An overlay is made on which all grains are numbered. Grain orientations are measured with the five axis universal stage, and orientations of the measured grains are calculated with the aid of a computer program (adapted from FABRIC I, Möckel, 1970). The output of this program gives the grain numbers, and orientations of α, β and γ_{ol} in ϱ and φ (see Möckel, 1969 p. 92) on a lower hemisphere projection.

Separate AVA diagrams for α, β and γ_{ol} can be constructed on drawings of the selected area. Individual grains are shaded or coloured differently, depending on their deviation from a chosen reference orientation (e.g. the angle of a specific crystal direction with S_{myl}) (Fig. 9).

Together with the AVA diagrams the pole figure diagrams are produced to reveal the overall orientation pattern of the selected area.

MICROTEXTURES INVESTIGATED

In the matrix, microtextures are defined by distinct areas in which specific grain shapes and preferred crystallographic orientations occur. The following microtextures are distinguished:

A. matrix grains to the side of porhyroclasts (e.g. specimen AR 14B1);

B. spherical agglomerates of equiaxed grains around which S_{myl}, defined by more flattened grains, is curved (e.g. specimen AR 14A1);

C. the normal foam texture in the matrix, defined by equiaxed grains with many triple point junctions (e.g. specimen AR 137C);

D. aggregates defining a foam texture between two remnants of porphyroclasts (e.g. specimen AR 110A).

RESULTS AND DISCUSSION

A. *Matrix to the side of porphyroclasts (reduced strain area)* (Figs. 10–14)

By examining matrix grains surrounding a porphyroclast, two areas can be distinguished (Fig. 12).

The area beside the porphyroclast in the direction of the foliation plane can be regarded as an area of reduced strain (strain shadow effect), because the strong clast protected the area from a deformation as intense as in the normal matrix.

Area I covers the porphyroclast and the matrix grains directly bordering the clast in this zone of reduced strain. The area has a flattened shape approximately parallel to S_{myl}.

Area II covers all matrix grains outside area I, and consists of grains flattened parallel to S_{myl}.

Petrofabric analysis of these two separate areas shows the following results (Fig. 11).

Area I. Here α_{ol} is situated in a girdle distribution with strong submaxima near S_{myl}, and a weaker maximum perpendicular to S_{myl}. γ_{ol} is distributed in a girdle pattern with submaxima in S_{myl}, and perpendicular to S_{myl}. β_{ol} does not deviate from the overall β_{ol} orientations in the matrix, and is situated in submaxima in a girdle pattern along S_{myl}.

Area II. Here α_{ol} shows a strong pointmaximum perpendicular to S_{myl}. The orientations of β_{ol} together with γ_{ol} form a great girdle pattern with submaxima along S_{myl}.

Discussion. – The different microstructures in regions I and II exhibit different crystallographic orientation patterns (Figs. 12, 13), namely the γ_{ol} and α_{ol} fabrics. A progressive modification of the fabric of area I into the fabric of area II is postulated to occur in the form of similar areas progressively deformed.

The scalloped grain boundaries of the porphyroclasts and the straight boundaries with triple point junctions of the surrounding matrix, suggest a recrystallization process (Honeycombe, 1968; Ragan, 1969), growing inwards into the porphyroclast.

The matrix next to the clast in area I consists of equiaxed grains with orientations close to that of the porphyroclasts (γ_{ol} fabric, Chapter II). This suggests that these grains derive from recrystallization at the rims of the porphyroclast, and that the recrystallization proceeds without a marked change in orientation. Subsequent deformation then tends to rotate the crystal axes further and further away from the inherited orientation.

In area I, the recrystallized grains did not change their orientation as rapidly towards another deformation position, because they were situated in a strain-reduced region. In these areas the preferred orientation of the recrystallized grains remains similar to that of the porphyroclasts.

In area II another preferred orientation is dominant. This pattern, with α_{ol} perpendicular to S_{myl}, and γ_{ol} in S_{myl}, is the preferred orientation of the overall matrix grains (Chapter II). Area II, unprotected by the porphyroclast, has undergone higher strain. The grains rotated towards another deformation position, and have reached, in area II, the final orientation defining the α_{ol} fabric.

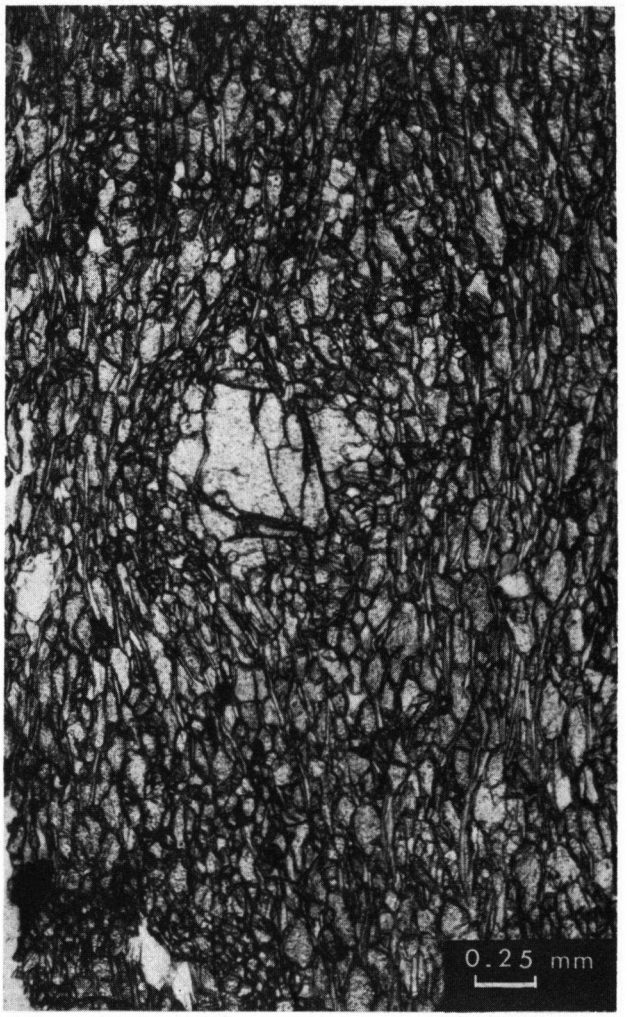

Fig. 10. Matrix to the side of porphyroclasts – studied area, sample AR 14B1.

B. *Spherical agglomerates* (Figs. 15–18)

In the matrix, spherical agglomerates of equiaxed grains occur (area I), surrounded by more flattened grains (area II) (Fig. 17).

There are differences in preferred orientation between these two areas.

In area I, α_{ol} is arranged in a great circle distribution normal to S_{myl}, with submaxima near S_{myl} and πS_{myl}. In contrast, in area II, there is a distinct pointmaximum of α_{ol} close to πS_{myl}. The orientation of β_{ol} is the same in both areas: an elongated pointmaximum in a girdle parallel to S_{myl}. γ_{ol} is in both areas dispersed with submaxima along S_{myl} and close to πS_{myl} (Fig. 16).

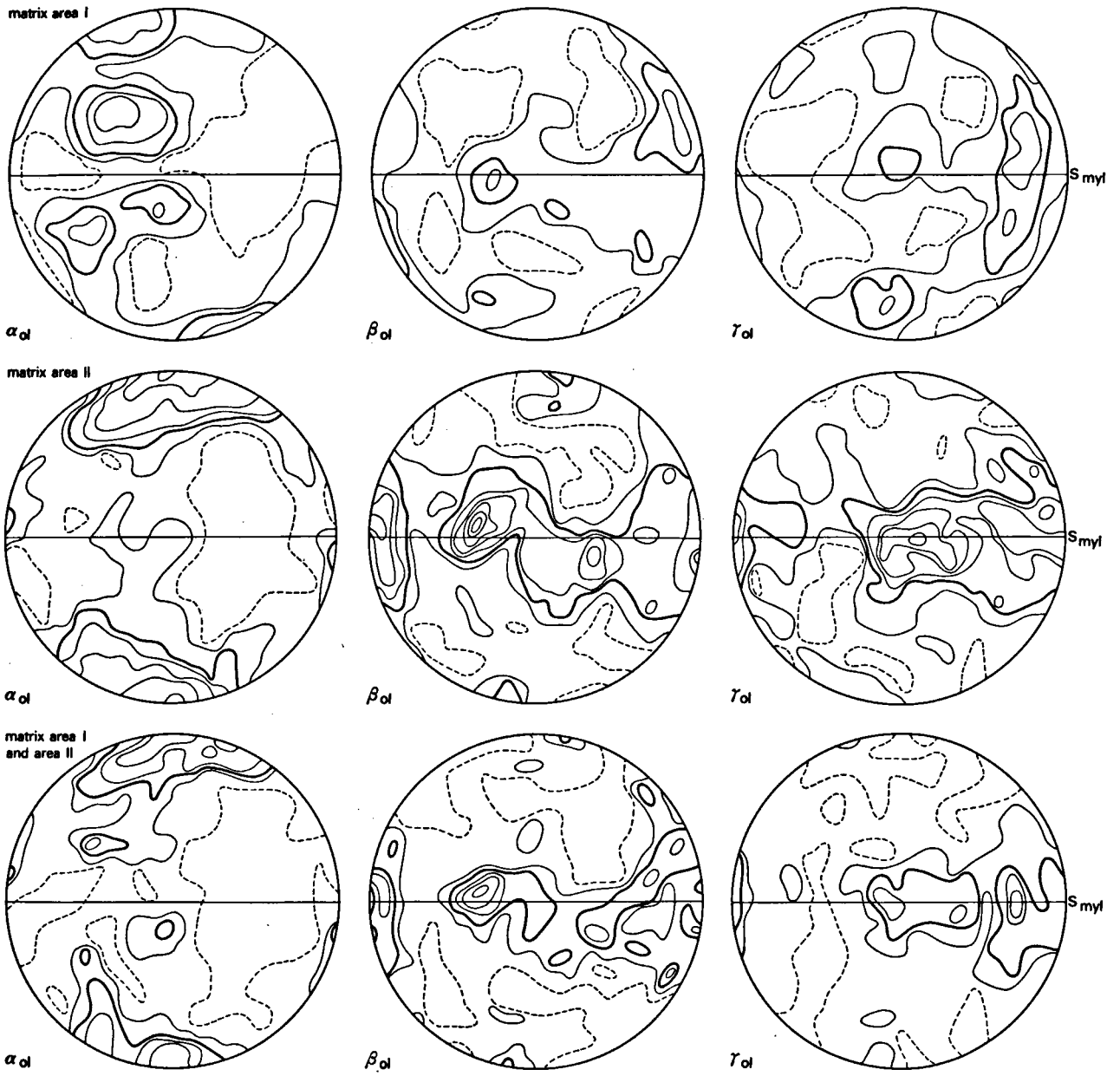

Fig. 11. Diagrams for the matrix to the side of porphyroclasts in AR 14B1 – area I olivine matrix: $N=79$, $A=0.04$; area II olivine matrix: $N=214$, $A=0.02$; area I and area II: $N=293$, $A=0.01$; contours at 1, 3, 5, 7, 9, 11, 13, 15 (for α_{ol} in area II, and area I and area II contours at 1, 3, 5, 7, 11, 17, 25).

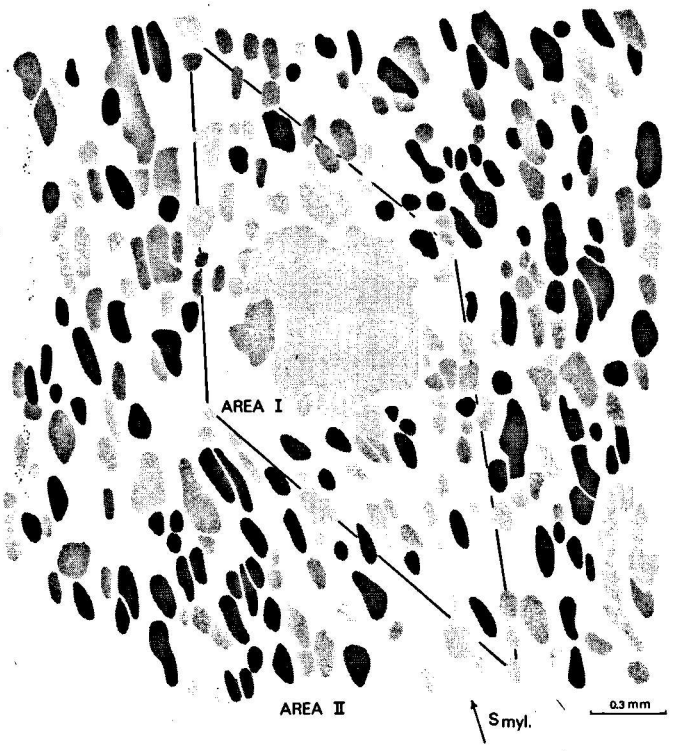

Fig. 12. Matrix to the side of porphyroclasts – the distribution of alpha-olivine, key shading Fig. 9.

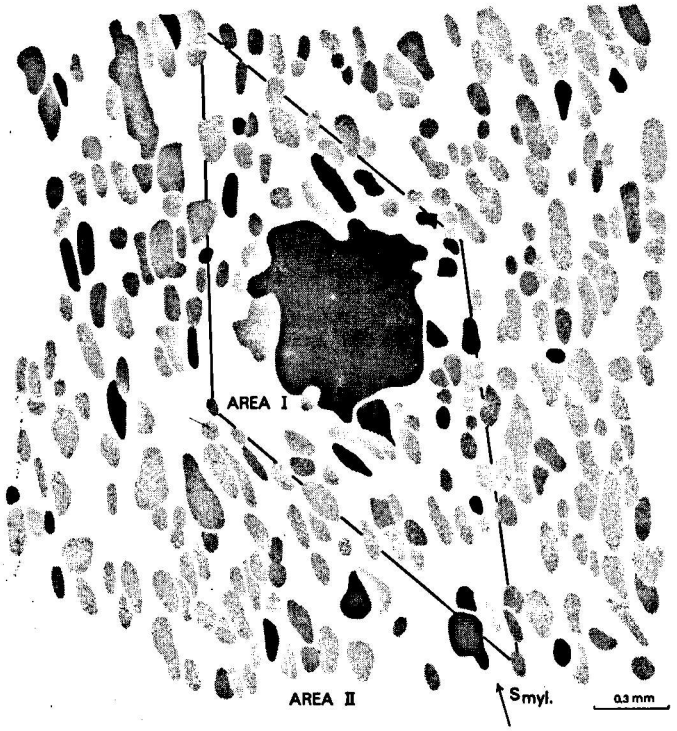

Fig. 13. Matrix to the side of porphyroclasts – the distribution of gamma-olivine, key shading Fig. 9.

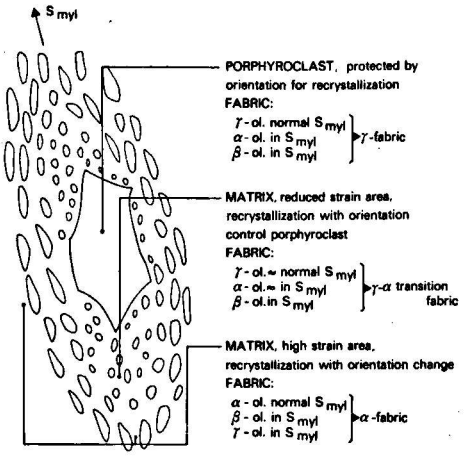

Fig. 14. Fabric development in matrix grains to the side of porphyroclasts.

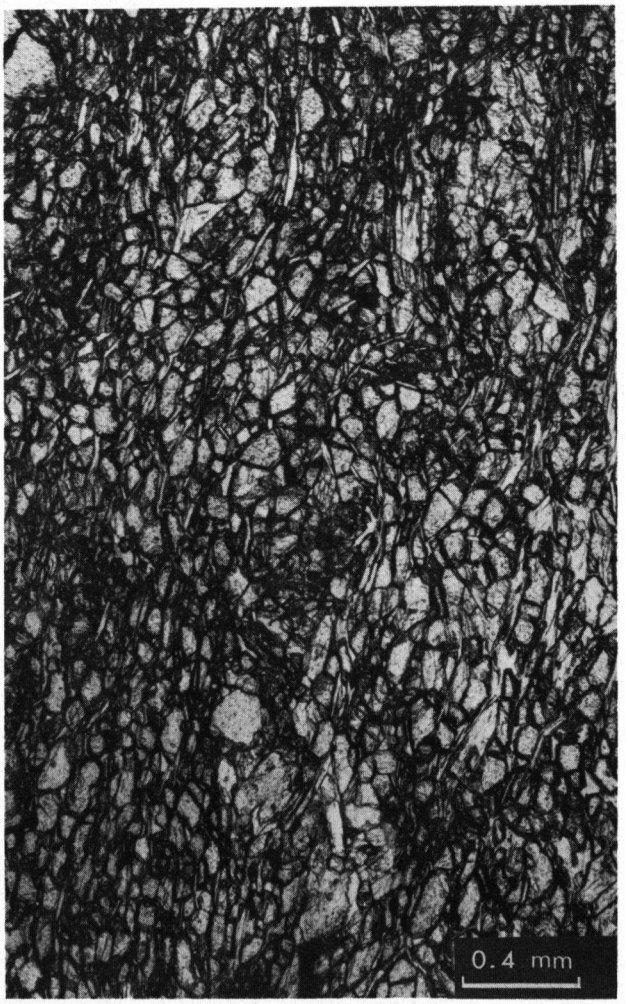

Fig. 15. Spherical agglomerates – studied area, sample AR 14A1.

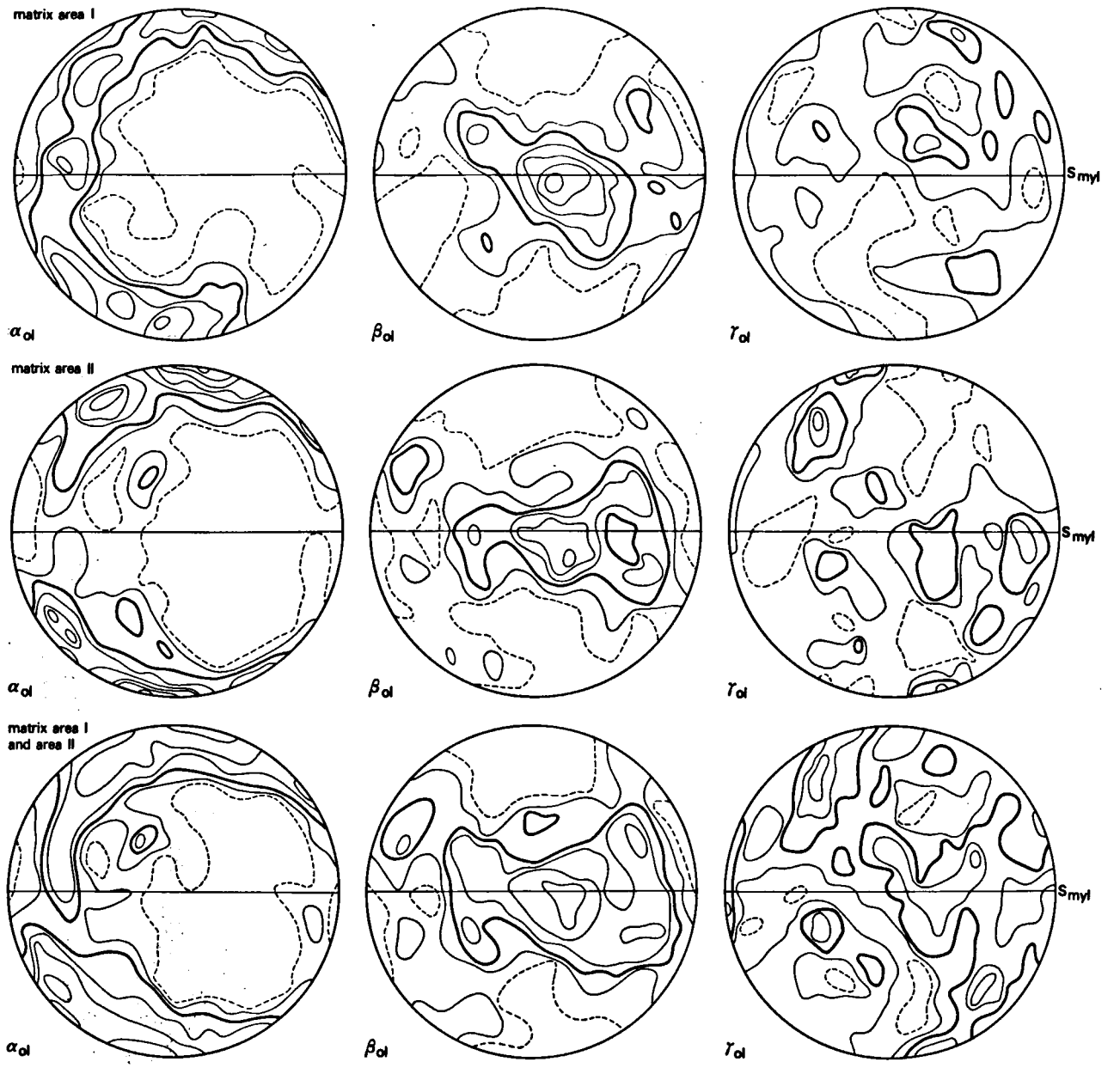

Fig. 16. Diagrams for the spherical agglomerates in AR 14A1 – area I olivine matrix: $N = 84$, $A = 0.04$; area II olivine matrix: $N = 160$, $A = 0.02$; area I and area II: $N = 244$, $A = 0.02$; contours at 1, 3, 5, 7, 9, 11, 13, 15 (for α_{ol} and β_{ol} in area I, and area II contours at 1, 3, 5, 7, 11, 17).

Fig. 17. Spherical agglomerates – the distribution of alpha-olivine, key shading Fig. 9.

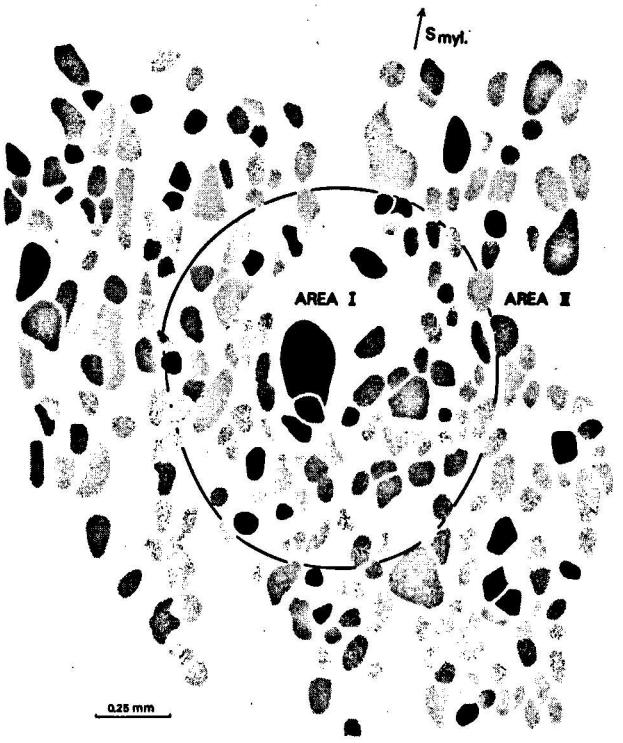

Fig. 18. Spherical agglomerates – the distribution of gamma-olivine, key shading Fig. 9.

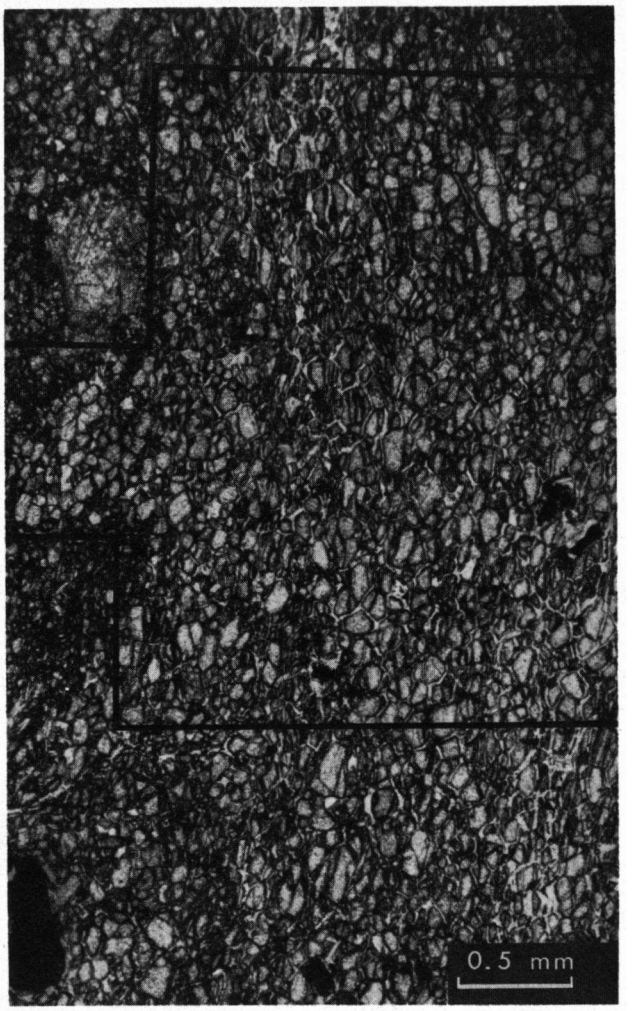

Fig. 19. The normal foam texture in the matrix – studied area, sample AR 137C.

Discussion. – It is suggested that the spherical agglomerates (area I) are replaced porphyroclasts. In area I, the influence of the replaced porphyroclast is only visible in the characteristic shape fabric (equiaxed grains) and some control of the crystallographic orientation of these grains, in that the orientation of the grains does resemble the preferred orientation of the porphyroclasts as a whole (the γ_{ol} fabric).

The orientation of the flattened matrix grains in area II has similarities with the main matrix fabric (the α_{ol} fabric), although especially γ_{ol} orientations deviate from the expected distribution parallel to S_{myl}.

Electron microscopy (Part II) did not indicate different types of large matrix grains, therefore the two distinct preferred orientation patterns in area I and area II can not be explained by different slip systems operative in these areas.

Once the stronger porphyroclast was replaced, the difference in strain response between areas I and II has been reduced. The grains in area I have undergone more strain

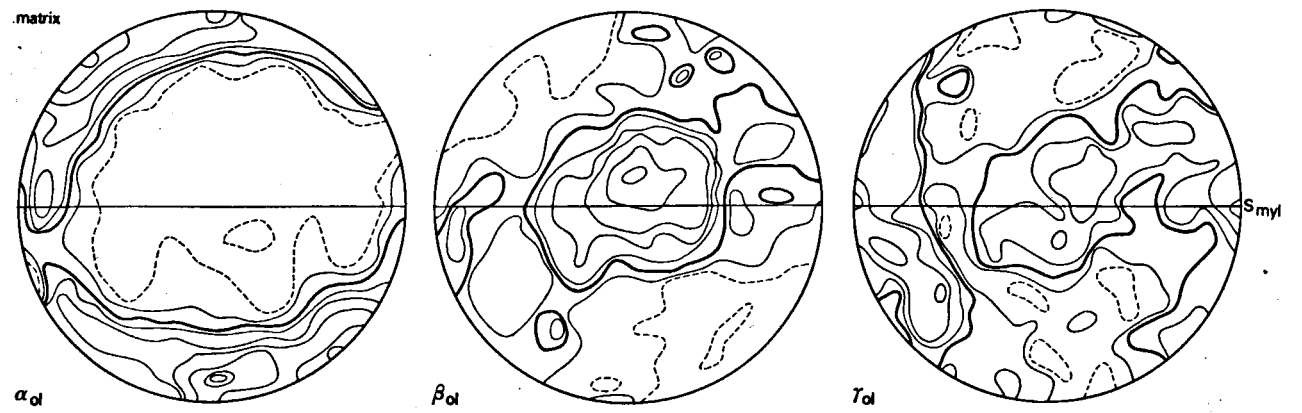

Fig. 20. Diagrams for the normal foam texture in the matrix in AR 137C – olivine matrix: $N = 585$, $A = 0.01$; contours at 1, 3, 5, 7, 11, 17, 25, 33, 39.

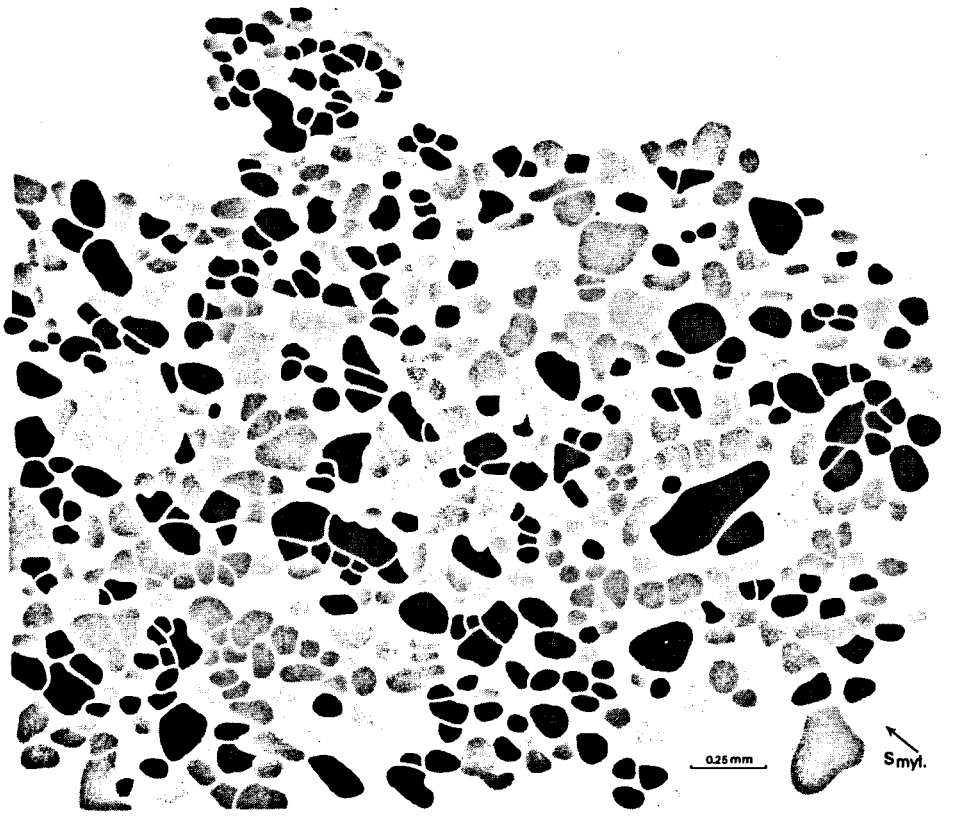

Fig. 21. The normal foam texture in the matrix – the distribution of alpha-olivine, key shading Fig. 9.

than in the previous example (Chapter IIIA), and consequently they rotated further away from the unstable γ_{ol} orientation. However, the grains in area I have not been strained considerably so soon after recrystallization of the porphyroclast, but have only started to reorientate towards the α_{ol} fabric. The orientations of the grains in area I are not the same as those of the replaced porphyroclast, but grade into the main matrix orientation (girdle fabric), because some deformation is undergone.

The fabric is transitional between the former porphyroclast orientation and the main matrix orientation, since the area has not been deformed sufficiently to produce the α_{ol} fabric. Further away from the replaced porphyroclast (area II), the deformation was sufficient to produce similarities with the final stage α_{ol} fabric in the matrix.

C. *The foam texture (area of highest strain)* (Figs. 19–22)
Distinct areas can not be separated, but the AVA gives an overall picture of the matrix fabric.

The area chosen can be regarded as situated in a relatively homogeneously strained region, because the porphyroclasts causing overall strain deviations in the surrounding matrix (Chapter IIIA, IIID), are absent.

The S_{myl} is difficult to define in this part of the thin section, because all grains are more or less equiaxed, forming the foam texture mentioned above. In other parts of the thin section the matrix is flattened, and S_{myl} can be reconstructed for the investigated area by using this orientation.

The crystallographic fabric similar to the main matrix orientation (the α_{ol} fabric), was earlier assumed to represent a final stage fabric development (Chapters II, IIIA).

The foam texture together with the strong preferred crystallographic orientation appears to represent the final product in the deformation process, in balance with the existing deformation conditions.

The foam textured matrix with more equiaxed grains, has in general the same preferred orientations as the more flattened grains in other regions. In both microtextures the

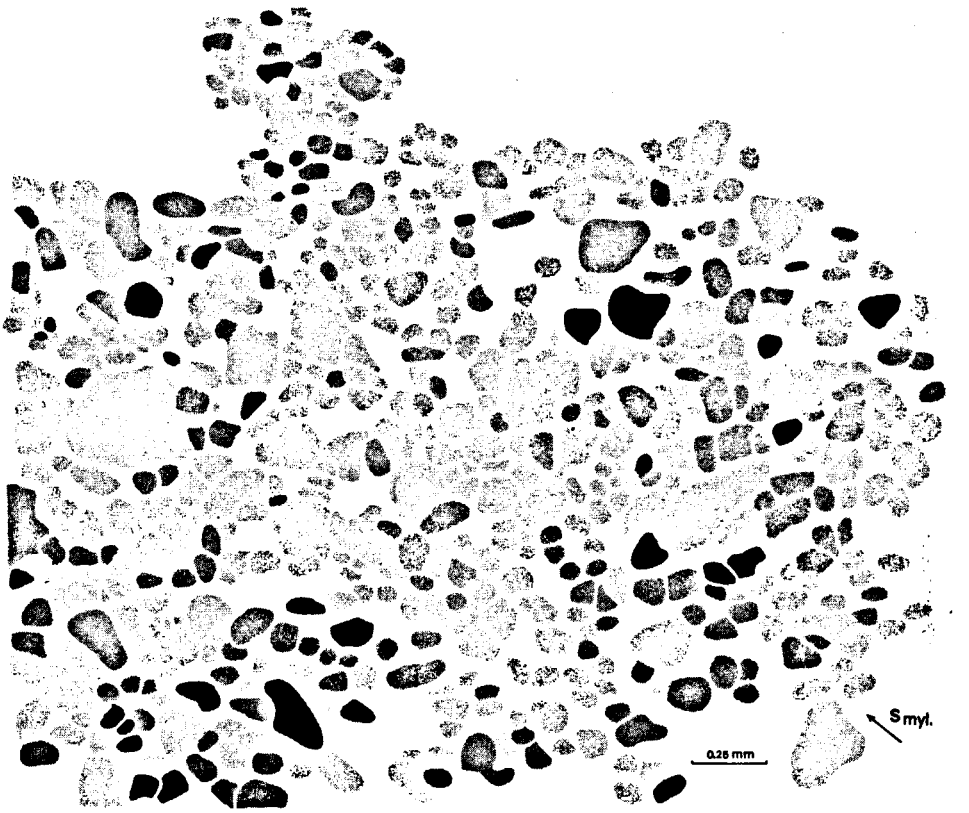

Fig. 22. The normal foam texture in the matrix – the distribution of gamma-olivine, key shading Fig. 9.

The distribution of the preferred orientations of α_{ol}, β_{ol} and γ_{ol} in the area is uniform and follows the trend of the main matrix fabric (α_{ol} pointmaximum close to πS_{myl}; γ_{ol} in S_{myl}). In general the deviations from the perfect α_{ol} fabric are slight. Although α_{ol} shows a pointmaximum parallel to πS_{myl}, distributions in a great circle towards S_{myl} are developed. γ_{ol} has submaxima in S_{myl}, and at low angles to S_{myl} (Fig. 20).

Discussion. — The shape fabric of equiaxed grains with triple point junctions points to a microstructure in which the grain boundary free energy was minimized (Honeycombe, 1968; Ragan, 1969; Stanton, 1972), situated in this microtexture in a high strain regime.

final fabric stage has been reached. The α_{ol} fabric is established in the foam texture, as the most unfavourable position for continued operation of the glide system for coaxial strain in a homogeneous high strain regime.

D. *A foam texture between two porphyroclasts* (Figs. 23–27) An area (I) of polygonal equiaxed matrix grains (ø up to 0.3 mm) between two porphyroclasts or remnants of clasts, is compared with surrounding matrix grains (ø up to 0.1 mm) of a more flattened habit (area II) (Fig. 25).

Fabric diagrams show a significant difference of orientation between these two distinct areas (Fig. 24).

The orientation of α_{ol} in area I is a strong pointmaximum in S_{myl}, while α_{ol} in area II shows a girdle pattern per-

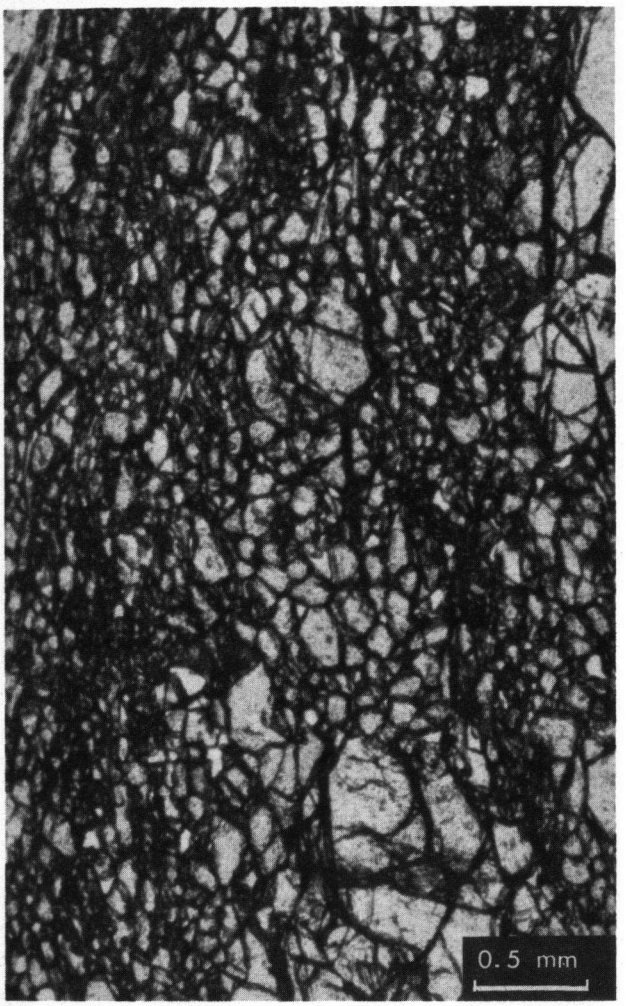

Fig. 23. The foam texture between two porphyroclasts – studied area, sample AR 110A.

pendicular to S_{myl} with a distinct pointmaximum at πS_{myl}. β_{ol} does not show different orientations in the separate areas. γ_{ol} shows a strong pointmaximum at πS_{myl} in area I, while γ_{ol} in area II shows a more dispersed arrangement with numerous submaxima, in general concentrated along S_{myl}, or at low angles to S_{myl}.

Discussion. – Area I forms a region protected from strain by two strong porphyroclasts (strain shadow effect), while area II was strained (Fig. 27). The differences observed in preferred orientations between the two areas can be related to differences in strain undergone during deformation.

Area II shows the main matrix distribution (the α_{ol} fabric). As already discussed (Chapters II, IIIA, IIIB), the fabric in area II is the expected fabric in the high strain regime.

The overall orientation in area I gives the same distribution as in the porphyroclasts (the γ_{ol} fabric), and deviates little from a single crystal orientation. Compared with the microstructure around a single porphyroclast (Chapter IIIA), the area I between the two clasts is an even better strain protected area. For this reason the inherited γ_{ol} fabric in area I remained strong after recrystallization; there was no need for the grains to reorientate into another deformation position.

The difference in grain size between area I (0.3 mm) and area II (0.1 mm) also indicates a protected region with a larger grain growth than in the strained area II.

GENERAL CONCLUSIONS

1. Recrystallization produced smaller grains from the larger porphyroclast (cf. processes described by Ardell et al., 1973, and White, 1975).
2. There is a progressive recrystallization. This is suggested by the increase in matrix grain diameter from small (0.03 mm) to larger (0.1 mm) values in areas respectively close to the porphyroclasts, and areas further away from them.
3. Recrystallization was related to the amount of deformation. Strain reduced areas next to the porphyroclasts exist because the clasts were harder to deform.
4. There is a progressive modification of the fabric as the amount of strain undergone increases from just recrystallized, equiaxed grains with a strong orientation control inherited from the porphyroclasts, to commonly flattened grains with a new orientation with respect to the strain axes.
5. The girdle patterns present in the matrix (Table 2, type B) are due to the bulk sampling method, which mixes different grain populations. Refined analysis of the girdle patterns shows a division into submaxima connected with defined grain populations in different strain regimes.

THE FABRIC DEVELOPMENT IN THE MYLONITE

In the mylonite a sequence of microstructures, connected with different preferred orientations, can be distinguished, suggesting progressive fabric development (Fig. 28).

In the chlorite peridotite, several zones of intense shear are developed, causing a deformation of the homogeneous, coarse grained rock into the mylonite. During this deformation a recrystallization process started at the grain boundaries of the porphyroclasts, forming small equidimensional olivine grains. Variable strain conditions in the mylonite developed either equiaxed grains or more flattened grains as matrix material. At this stage three types of grains existed in the material:

1. the porphyroclasts as remnants;
2. the equiaxed to flattened grains in the matrix in high strain regimes;
3. the equiaxed matrix grains in reduced strain regimes.

These three types of grains also have different preferred orientations, and define specific microtextures.

The porphyroclasts, with the starting fabric γ_{ol} perpendicular to S_{myl}, and α_{ol} in S_{myl}, show all kinds of transitions in great circle distributions of γ_{ol} towards S_{myl}, and α_{ol} towards πS_{myl}. This fabric development points to a rotation of the porphyroclasts from a position hard to deform (the γ_{ol} fabric), into positions of the main matrix orientation (the α_{ol} fabric).

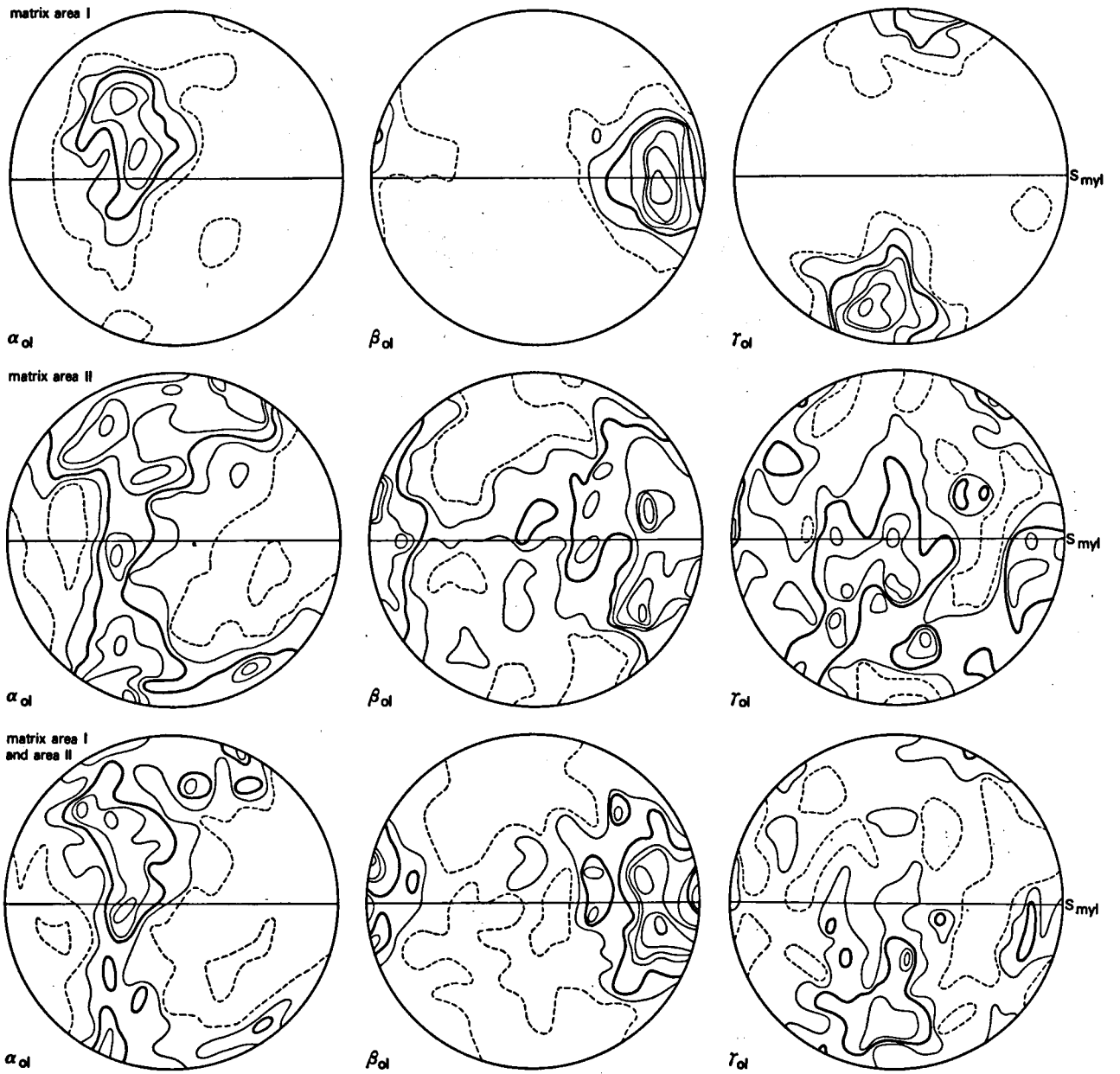

Fig. 24. Diagrams for the foam texture between two porphyroclasts in AR 110A – area I olivine matrix: $N = 77$, $A = 0.02$; area II olivine matrix: $N = 211$, $A = 0.02$; area I and area II: $N = 288$, $A = 0.01$; contours at 1, 3, 5, 7, 9, 11, 13.

The matrix grains in high strain regimes have preferred orientations leading to a rotationally stable deformation orientation; they could not or did not want to change: α_{ol} perpendicular to S_{myl}, and β_{ol} together with γ_{ol} in S_{myl}. These grains, forming foam textures (triple point junctions), can be regarded as a final stage in fabric development, with a uniform preferred orientation, well-balanced to the strain axes (the α_{ol} fabric).

The equiaxed grains in strain reduced zones occupy a position concerning habit and location, between the grains in high strain regimes and the porphyroclasts. These grains possess transitional preferred orientations still related to the clast orientations because rotations towards another deformation position were still small. The equiaxed grains with these preferred orientations can be regarded as forming transitional fabrics, situated in low strain areas

Fig. 25. The foam texture between two porphyroclasts – the distribution of alpha-olivine, key shading Fig. 9.

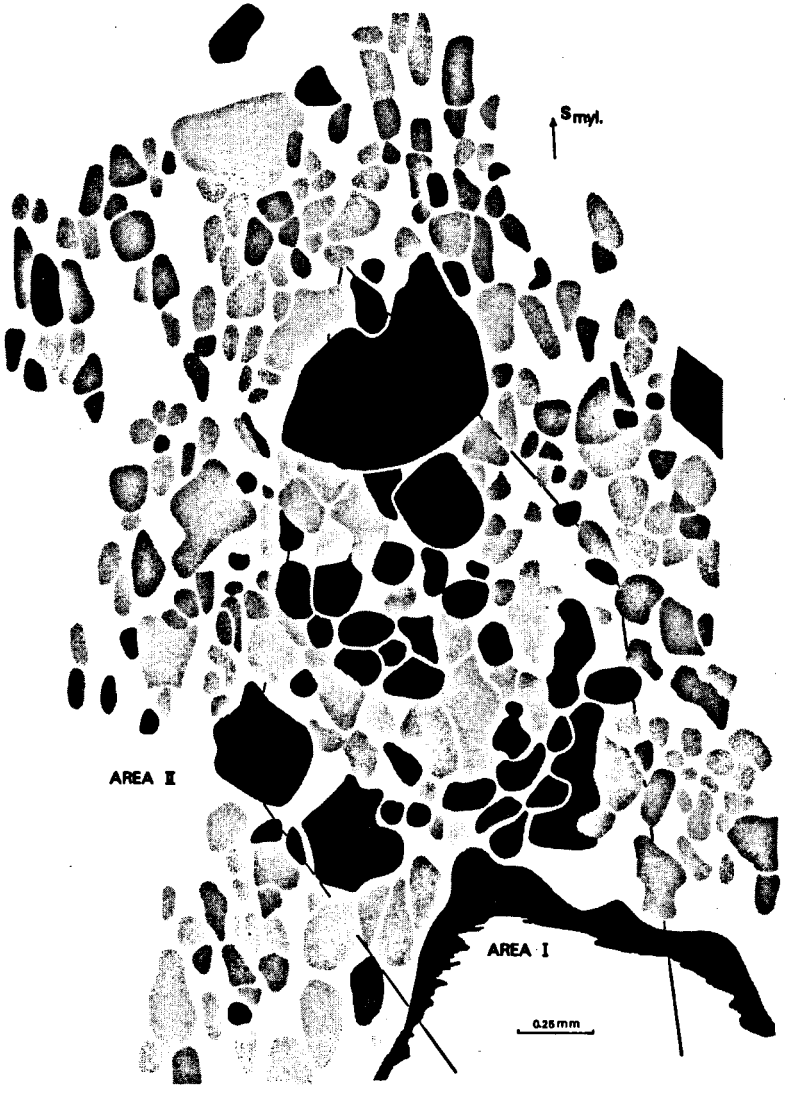

Fig. 26. The foam texture between two porphyroclasts – the distribution of gamma-olivine, key shading Fig. 9.

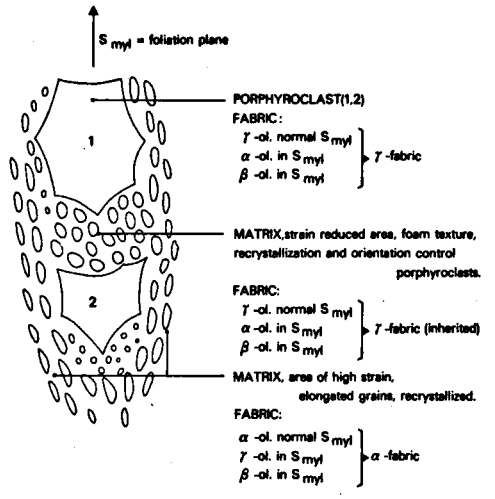

Fig. 27. Fabric development in the foam texture between two porphyroclasts.

(Chapter IIIA, IIID) or in areas only just fully exposed to the strain (Chapter IIIB), but with a strong preferred orientation inherited from the replaced porphyroclasts.

The following succession in fabric development in the mylonite is proposed (Fig. 28):

1. porphyroclasts are rotated and recrystallized at their rims (microtexture Chapter IIIA, IIID);
2. recrystallization continues until the entire porphyroclast is replaced by an equiaxed matrix, producing spherical agglomerates (microtexture Chapter IIIB);
3. the fabric of the spherical agglomerates, still related to the recrystallized porphyroclast, grades into the ideal matrix texture (e. g. microtexture Chapter IIIC, or a flattened matrix).

This sequence of events is proposed for the development of the shape and crystallographic fabrics in the mylonite.

In general it can be concluded that in areas of small strain, the recrystallized matrix possesses preferred orientations related to the clasts, resulting in transition fabrics. These grains only have undergone small rotations towards the other position, relative to the strain axes.

Depending on the deformation process, the grains in recrystallizing matrix in areas of high strain, rotated either towards the most unfavourable position for continued operation of dislocation glide in coaxial strain, or towards a more favourable position for continued operation of dislocation glide in the case of a simple shear deformation, resulting both in the present α_{ol} fabric.

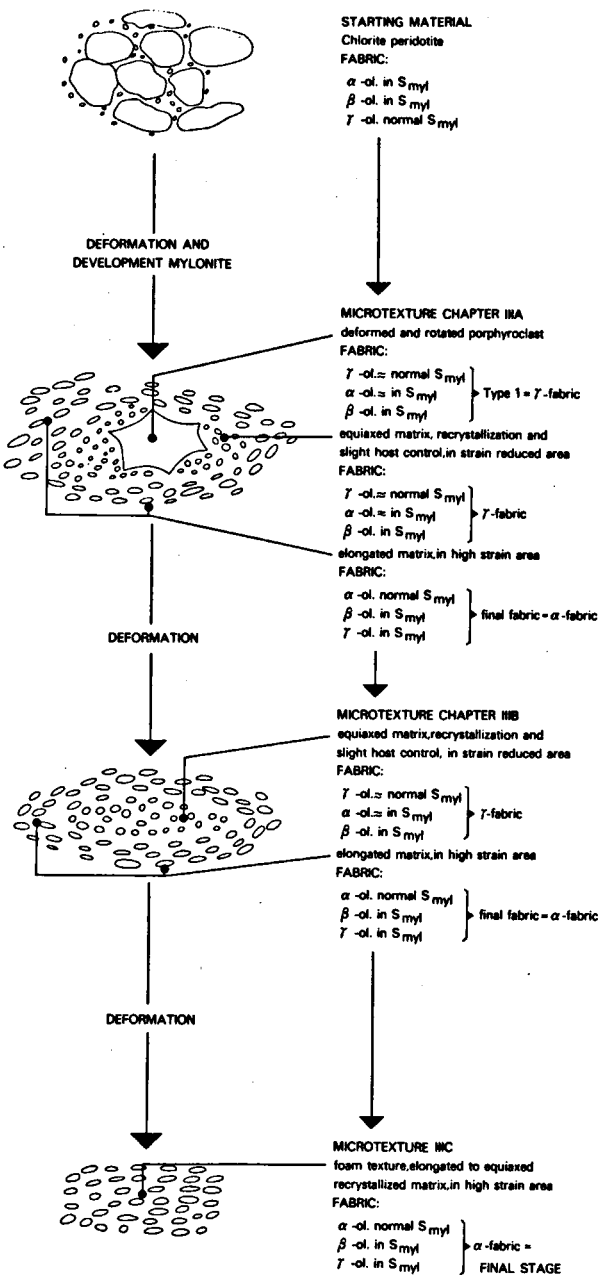

Fig. 28. The fabric development in the mylonite.

PART II

CHAPTER I

HIGH VOLTAGE ELECTRON MICROSCOPY OF THE MYLONITE

INTRODUCTION

High voltage electron microscopy (HVEM) is used to refine the optical microscopy, and to get a better insight into the deformation mechanisms responsible for the formation of the mylonite (Buiskool Toxopeus & Boland, 1976). The dislocation substructures have been correlated with the deformation mechanisms known to be operative in metallic and ceramic systems, and hence an estimate of the conditions of deformation can be made. An attempt is made to establish a relationship between the dislocation substructures and the different textural units recognized in the mylonite.

The microscopy was performed on the AEI-EM7 electron microscope, operating at one million volts (1 MeV), in the Department of Metallurgy and Science of Materials in Oxford, England.

Techniques for specimen preparation (see Barber, 1970; Gillespie et al., 1971) and Burgers vector determination (see Hirsch et al., 1965; Head et al., 1973; Steeds, 1973; Boland, 1976) are not discussed in this paper.

All data used, have been compiled from several hand-specimens, thin sections and differently oriented foils examined in the HVEM.

Before attempting to correlate dislocation arrangements with the deformational history, it should be emphasized that the dislocation arrangements most probably reflect the last thermal or dynamic metamorphic event or episode. Thus the effects of prior events will have been modified to an extent dependent on the conditions of this last event.

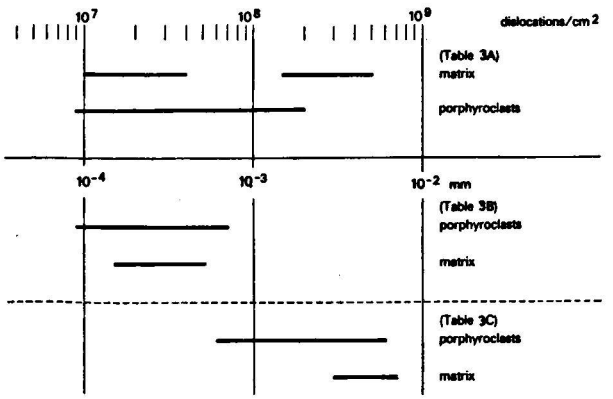

Table 3. A – dislocation densities;
B – spacings between dislocations within (100) edge dislocation arrays;
C – spacings between (100) edge dislocation arrays.

OBSERVATIONS

The porphyroclasts (Table 3)

See Buiskool Toxopeus & Boland, 1976. The most striking feature of the dislocation arrangement is the regular succession of closely spaced (0.6 to 6.0 um) arrays of dislocations (Fig. 29; and in Buiskool Toxopeus & Boland, 1976, fig. 6A). The (100) arrays consist of edge dislocations with Burgers vector **b** = [100], in symmetrical tilt boundary arrangement. The dislocation spacings within the arrays vary from 0.09 to 0.7 um. The dislocation directions are variable per array, giving rise to pseudo 'loop-type' structures (Boland, 1974, fig. 1; Boland & Buiskool Toxopeus,

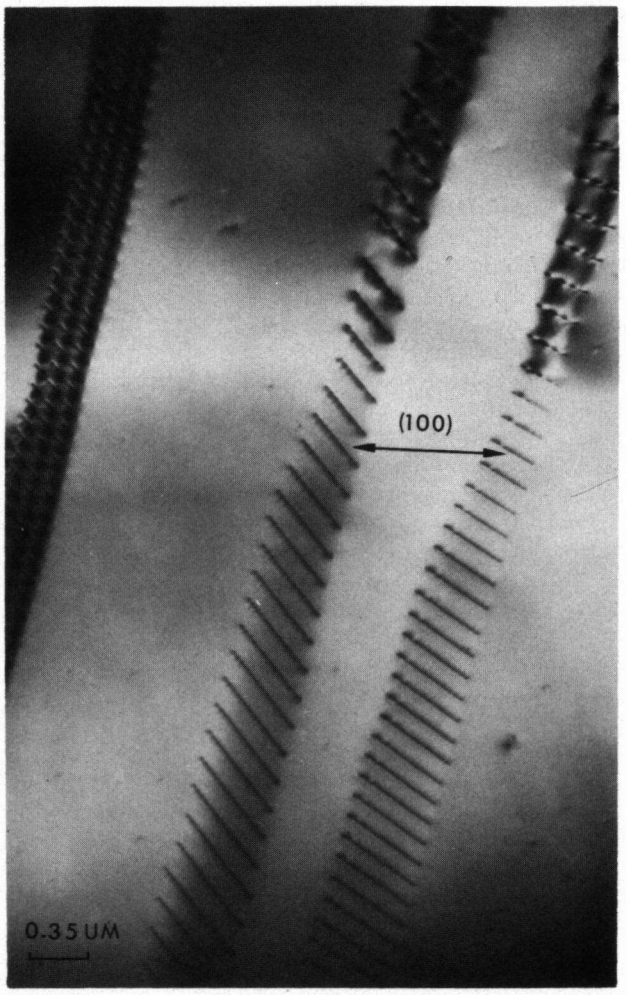

Fig. 29. Successive arrays of edge dislocations, **b** = [100], forming symmetrical low angle tilt boundaries in (100). Note the varying dislocation direction, **u**, per array (porphyroclast).

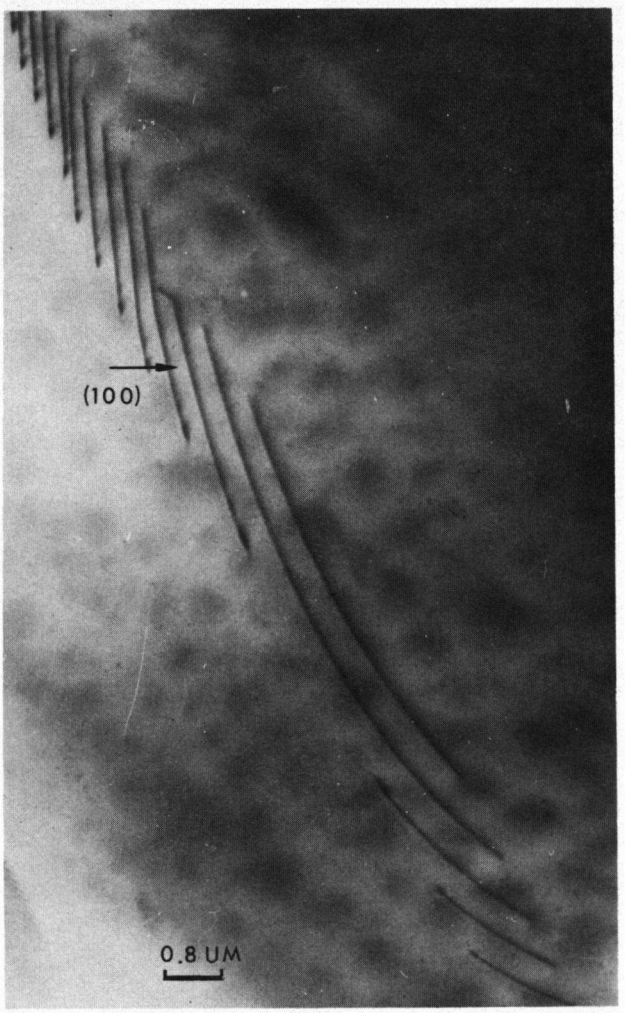

Fig. 30. Pseudo loop-type structures in (100) tilt boundaries (porphyroclast).

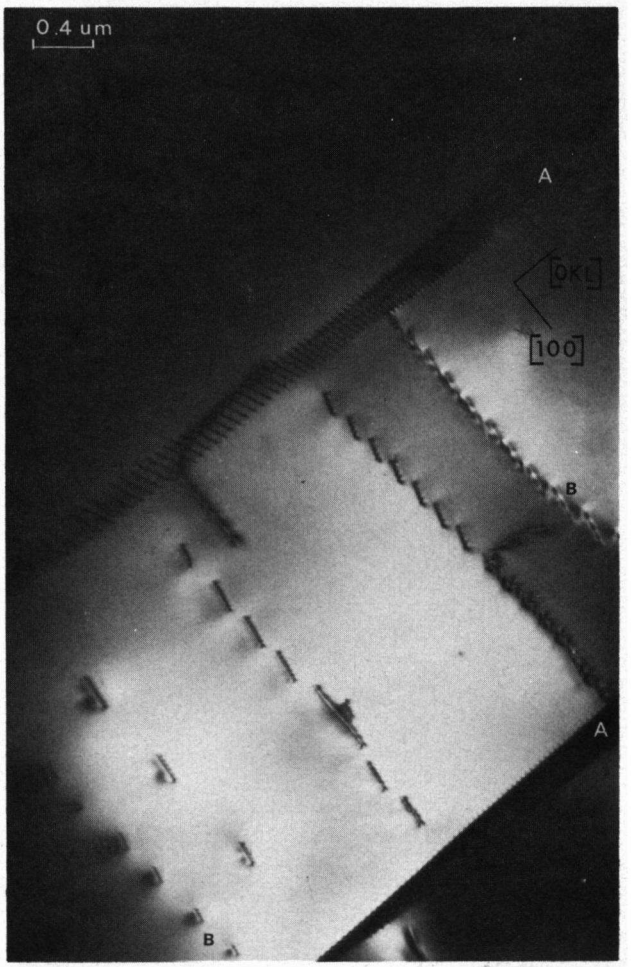

Fig. 31. Two symmetrical tilt boundaries (A) composed of $\mathbf{b} = [100]$ edge discolations in (100), with cross arrays (B) of edge dislocations $\mathbf{b} = [100]$ in {0kl} in slipplane configuration (porphyroclast).

1974) (Fig. 30). A common feature in the (100) arrays is the 'bowing out' of some dislocations into (001) to produce screw dislocation arrays (Buiskool Toxopeus & Boland, 1974, figs. 4, 5). Less frequently observed are cross arrays of edge dislocations with $\mathbf{b} = [100]$, being of the general form {0kl} (Fig. 31).

In addition to the dislocations located in arrays, free or individual dislocations are observed. Their density is low (9×10^6 to 2×10^8/cm^2); they are straight and, both in edge and screw type configurations, with $\mathbf{b} = [100]$ type predominating over the $\mathbf{b} = [001]$ type dislocations.

The matrix (Table 3)

The (100) arrays with Burgers vector $\mathbf{b} = [100]$ are also present, but with a larger, irregular spacing (greater than 3 um). The dislocation spacings in the (100) arrays do not reach very small values (0.15 to 0.5 um), while the dislocation directions in (100) have still the same variability as in the porphyroclasts. The 'bowing out' effect is observed while the frequency of cross arrays of $\mathbf{b} = [100]$ dislocations has markedly increased. The cross arrays parallel to (001) or (010) have dislocation directions $\mathbf{u} = [010]$ and $\mathbf{u} = [001]$ respectively. Twist boundaries composed of a square mesh of $\mathbf{b} = [001]$ and $\mathbf{b} = [100]$ screw dislocations in (010) or possibly more general {0kl} planes, are a common feature (Fig. 32).

The individual dislocations are inhomogeneously distributed within the crystals, with $\mathbf{b} = [001]$ dislocations predominating over $\mathbf{b} = [100]$. The dislocations with $\mathbf{b} = [100]$ are either straight and situated in (001) parallel to [010] or [100], indicating an edge and screw character respectively, or curved with a mixed screw/edge character in planes not strictly defined. The $\mathbf{b} = [001]$ dislocations are always straight, tending to group in dense bands (densities up to 5×10^8/cm^2). They can have directions parallel to [100] or [010], and thus have a pure edge character; $\mathbf{b} = [001]$ screw dislocations are also present.

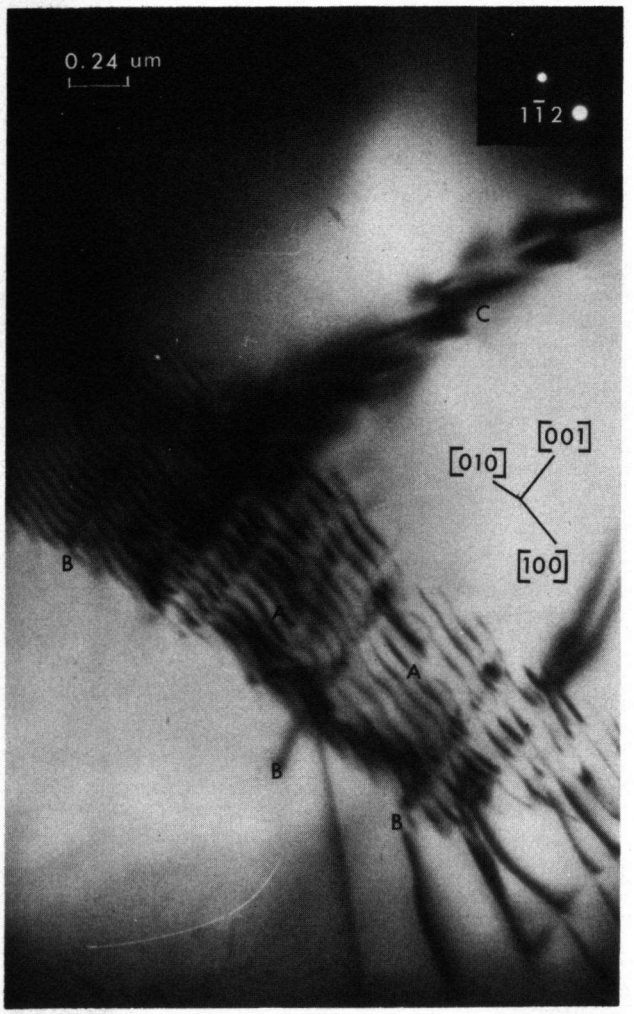

Fig. 32. A twist boundary in the matrix in (0kl) composed of $\mathbf{b} = [100]$ (A) and $\mathbf{b} = [001]$ (B) screw dislocations. Note the difference in contrast due to different $\mathbf{g} \times \mathbf{b} \wedge \mathbf{u}$ conditions (Figs. 39–42). (C) is a tilt boundary of $\mathbf{b} = [100]$ edge dislocations in (100).

DISCUSSION

The segmented undulatory extinction, observed optically in the porphyroclasts (Fig. 3), is directly related to the (100) dislocation arrays, identified in the HVEM as symmetrical tilt boundaries (see also Raleigh, 1968).

The orientation changes across the boundaries are directly related to the dislocation Burgers vector (**b**) and the spacing of the dislocations (h) by: $\mathbf{b}/h = 2 \sin \theta/2$; for small θ this reduces to $\theta = \mathbf{b}/h$ (Cottrell, 1953; Hull, 1965); θ is the angle of misorientation between the two parts of the crystal.

If $\mathbf{b} = [100]$, $|\mathbf{b}| = 4.76$ Å, and for a spacing of $h = 500$ Å, the misorientation to be expected is 0.55 degree. Values of the misorientation are commonly found to be less than one degree using both optical and selected area diffraction measurements across the boundaries. As the dislocation spacing increases, the angle θ is reduced and it may not be directly measureable by these techniques (Boland et al., 1971).

Because the kink or tilt boundaries may be as closely spaced as 0.6 um, the optical observations often fail to resolve individual boundaries (Boland et al., 1971).

In the optical microscope, individual, broadly spaced kink boundaries are measured with a five axes stage following the method described by Raleigh (1968). In all cases the boundaries are parallel to (100); however, it is often found that the apparent external rotation axis (ER) lies outside the (100) plane (Fig. 33). These deviations of the ER from the (100) plane are the result of small, unavoidable errors in the orientation measurements of the crystal parts on both sides of the boundary, due to the inaccuracy of the optical measuring technique.

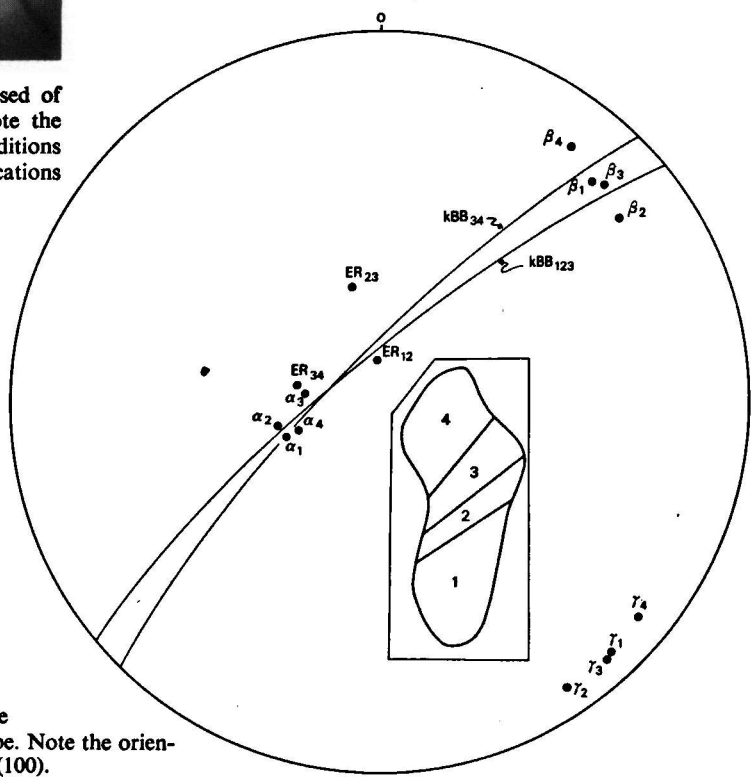

Fig. 33. A set of kink bands parallel to (100) of an olivine porphyroclast (inset) measured with the optical microscope. Note the orientation deviations of the external rotation axes (ER) from (100).

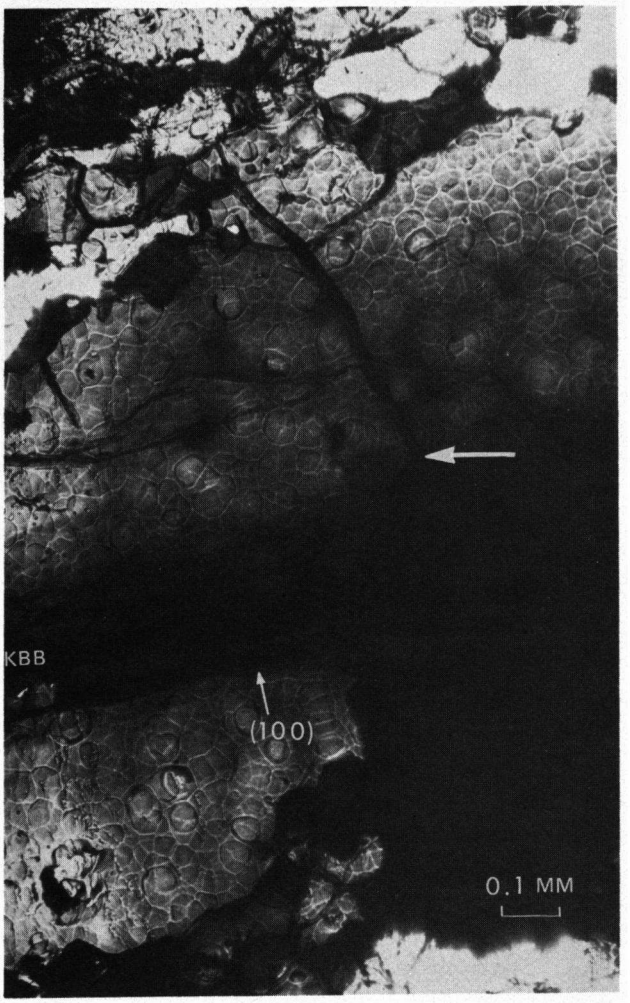

Fig. 34. Kink boundaries (KBB) parallel to (100) in an edge of an ion-beam thinned olivine porphyroclast. Optical photograph with crossed nicols.

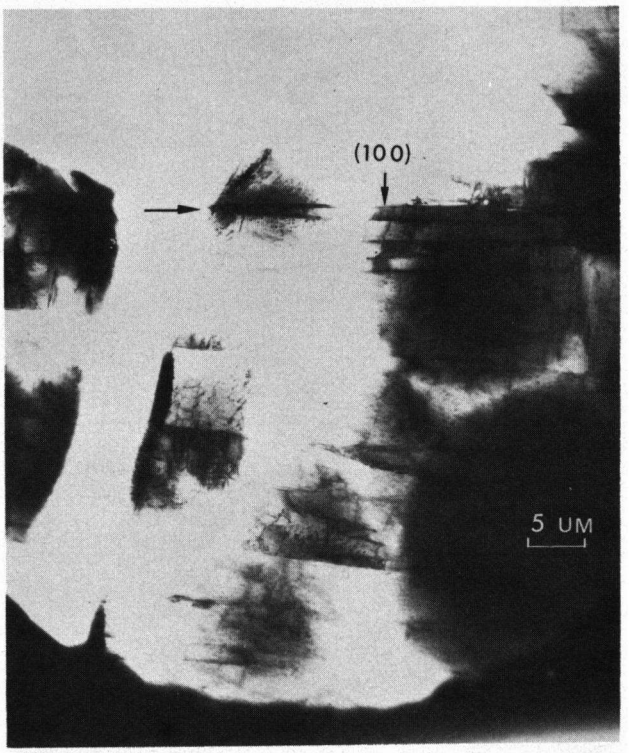

Fig. 35. The same area as Fig. 34 in the HVEM lowest magnification. Kink boundaries are present as individual edge dislocation arrays, $\mathbf{b} = [100]$, parallel to (100).

A one to one correspondence between the (100) edge dislocation arrays, with $\mathbf{b} = [100]$, and the kink boundaries parallel to (100), has been established in this study (Figs. 34, 35 and 36) and also by Green & Radcliffe (1972b). In the optical microscope, however, a constant bending of the lattice by kink boundaries is not always visible; a more abruptly alternating extinction is commonly recorded (Fig. 3). The alternate bending in the lattice is the result of the change in sign of the edge dislocations per array.

The pseudo 'loop-type' structures (Fig. 30; and Buiskool Toxopeus & Boland, 1976, fig. 6B) are commonly recorded in orientations in which the (100) plane is inclined at high angles to the plane of the foil. Observations of a (100) section, which should give a more accurate picture of the dislocation arrangement in (100), never revealed the loop closure. The optical properties of the kink boundaries would be difficult to explain if the arrays were composed of concentric prismatic loops; it would imply a reverse of the undulatory extinction along the loop structure.

Dislocations are grouped into parallel alignments, although they did curve within the (100) plane (Fig. 37). It is obvious that these dislocations are responsible for the 'loop-type' structures reported earlier (Boland, 1974; Boland & Buiskool Toxopeus, 1974).

In those regions where the dislocations bowed out of the (100) plane into directions parallel to [100], marked curvature of the remaining dislocations is observed (Fig. 38). This curvature represents a rearrangement process of the dislocations, the driving force being the stress generated in those regions of variable dislocation spacing (h). The dislocations adjacent to the dislocations leaving (100), changed their directions in order to retain a constant spacing (the lowest energy situation; Cottrell, 1953).

Optical microscopy of an isolated kink boundary shows a constant misorientation across the array, and electron microscopy confirms this, but only by statistical averaging of the dislocation spacing over several micron lengths along the array.

In many instances, the dislocations that bow out of the (100) arrays follow quite definite crystallographic planes instead of a more curved direction. For example, the dislocations may change according to the following sequence (Buiskool Toxopeus & Boland, 1976, figs. 4, 5):

1. from the (100) plane into
2. the (101) plane into
3. the (001) plane, parallel to [100], into
4. the $(\bar{1}01)$ plane and finally back into
5. the (100) plane.

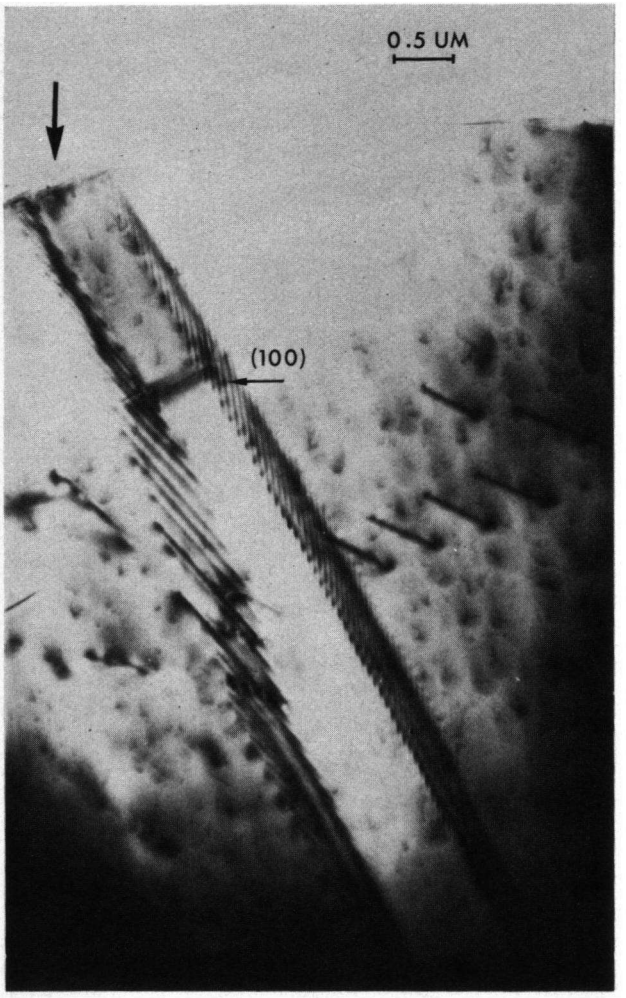

Fig. 36. A high magnification micrograph of an area present in Fig. 35 showing clearly the (100) subboundaries.

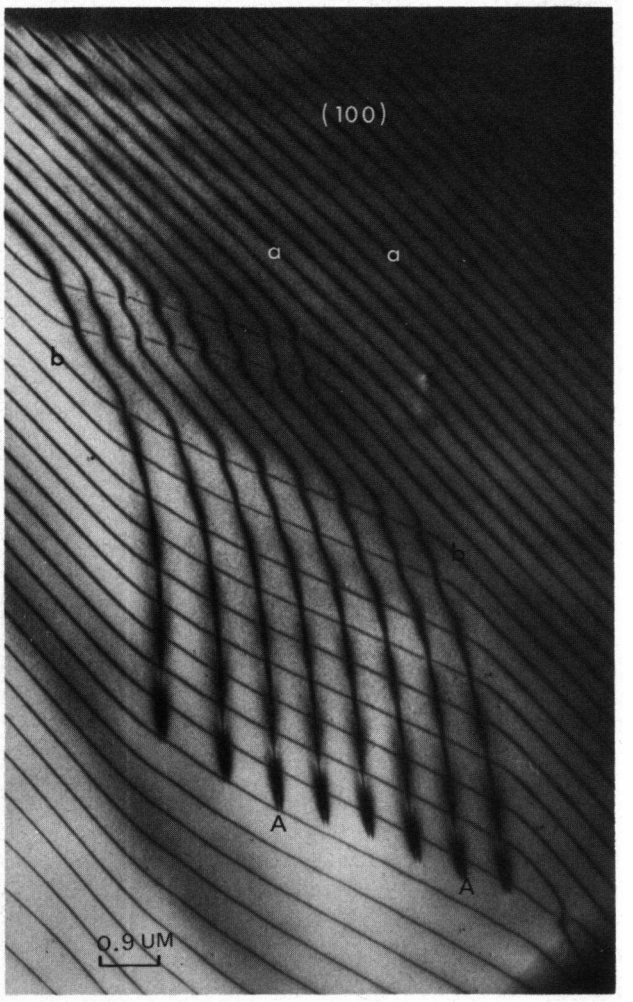

Fig. 37. Micrograph of a thin area parallel to a (100) tilt boundary. A set of dislocations (A) is bowing out of this plane. The edge dislocations remaining in (100) change their straight appearance (a) to curved directions (b) in (100), in order to retain their constant spacing; these curvatures form the pseudo loop structures (Fig. 30).

The bowing out of (100) of dislocations with $\mathbf{b} = [100]$, is attended by a change in character of the dislocations; from a pure edge type in (100) to a mixed screw/edge type in $\{101\}$, and to a pure screw type in (001). Under equilibrium conditions of the low internal energy within the grains, this crystallographic control of the dislocation direction indicates the minimum energy path of the dislocation. Although the evidence is as yet inconclusive (Boland & Hobbs, in prep.; Boland & Paterson, unpubl. observations), it does imply that the Peierl's stress is significant in olivine (Boland, 1974).

The pure screw dislocations in arrays parallel to (001) have larger spacings (several microns) than the edge dislocations in arrays parallel to (100) (less than 1 um). Therefore the array type arrangement formed in (001) can not be considered as an unstable type of boundary, although it forms a higher energy situation (Cottrell, 1953).

The arrays parallel to (100) and (001) form elongate subgrains parallel to [010]. These cells may be terminated by edge dislocation cross arrays in (010) or $\{0kl\}$ (see also Green & Radcliffe, 1972b, fig. 15). The porphyroclasts are therefore mosaics of subgrains, either flattened along (100) planes, or elongated parallel to [010]. The subgrain boundaries consist of symmetrical (100) tilt boundaries, edge dislocation cross arrays often in slip plane configuration (e.g. (001), (010), $\{0kl\}$), and screw dislocation arrays in (001).

Within the subgrains, there are low densities (about 10^7 to $10^8/cm^2$) of free or individual dislocations; they are generally straight, of edge and screw character with $\mathbf{b} = [100]$ predominating over $\mathbf{b} = [001]$ type dislocations.

There are significant differences between the dislocation substructures of the matrix and those in the porphyroclasts.

Fig. 38. Detail of Fig. 37 – dislocations (B) remaining in (100) curve at places where other dislocations (A) bow out of (100), in order to retain their constant spacing.

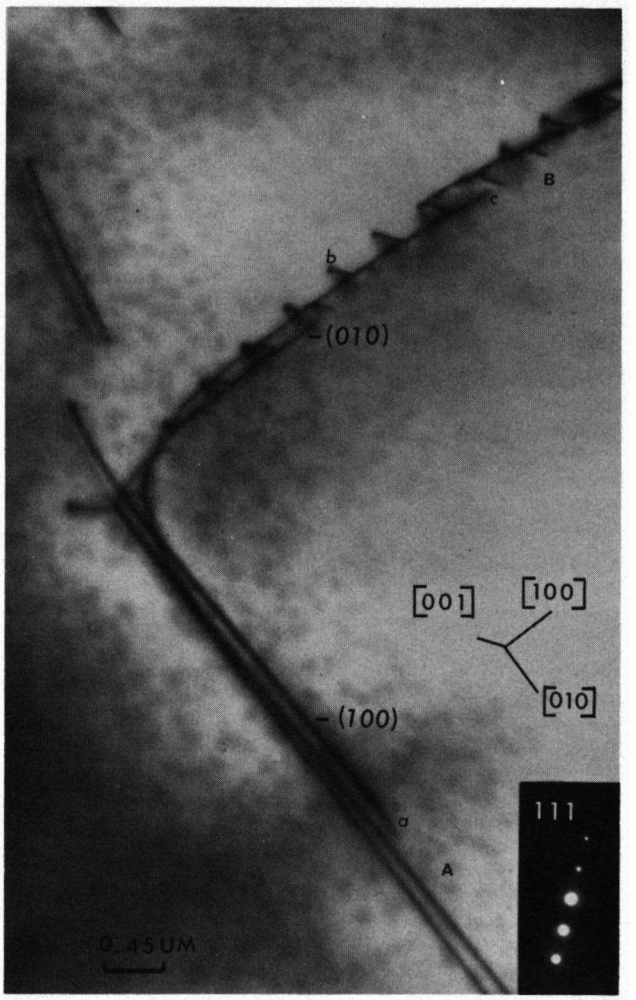

Fig. 39. A tilt boundary (A) in (100) is changing into a twist boundary (B) in (010). The edge dislocations (a) in (100) with $\mathbf{b} = [100]$ bow out into (010) forming screw dislocations (c). To reduce this high energy situation a second set of screw dislocations (b), with $\mathbf{b} = [001]$, is introduced in (010), forming the twist boundary (matrix).

These are:
1. (100) arrays of the matrix are more widely, but irregularly spaced (larger than 3 um);
2. there are numerous cross arrays in (001) and (010) composed of $\mathbf{b} = [100]$ edge dislocations, and
3. the presence of twist boundaries in (010) or more generally {0kl} (Figs. 39–42).

A change in direction of the tilt boundaries can result in a transformation from edge dislocation to screw dislocation arrays (Fig. 39). These screw dislocation arrays, with $\mathbf{b} = [100]$, are unstable (small dislocation spacing within the array). The introduction of a second set of screw dislocations, with $\mathbf{b} = [001]$, is necessary (Cottrell, 1953), giving rise to a twist boundary arrangement.

The above-mentioned three types of subboundaries define the larger subgrains (10 to 50 um) of the matrix (Figs. 43, 44). Along some tilt boundaries another small subgrain type (smaller than 5 um) has been observed. In contrast to the larger subgrains with dislocation densities as high as $5 \times 10^8/\text{cm}^2$, these smaller subgrains have no free dislocations, and appear to be bounded by high-angle grain boundaries composed of complex dislocation arrays (Gleiter & Chalmers, 1972). The significance of this feature is described below.

In contrast with the porphyroclasts, where the free dislocations are mainly of the $\mathbf{b} = [100]$ type, the matrix has a predominance of $\mathbf{b} = [001]$ free dislocations. This indicates that the dominant active glide systems vary from {0kl} [100] in the porphyroclasts, to (100) [001], (010) [001], (110) [001], and {0kl} [100] in the matrix (cf. Phakey et al., 1972).

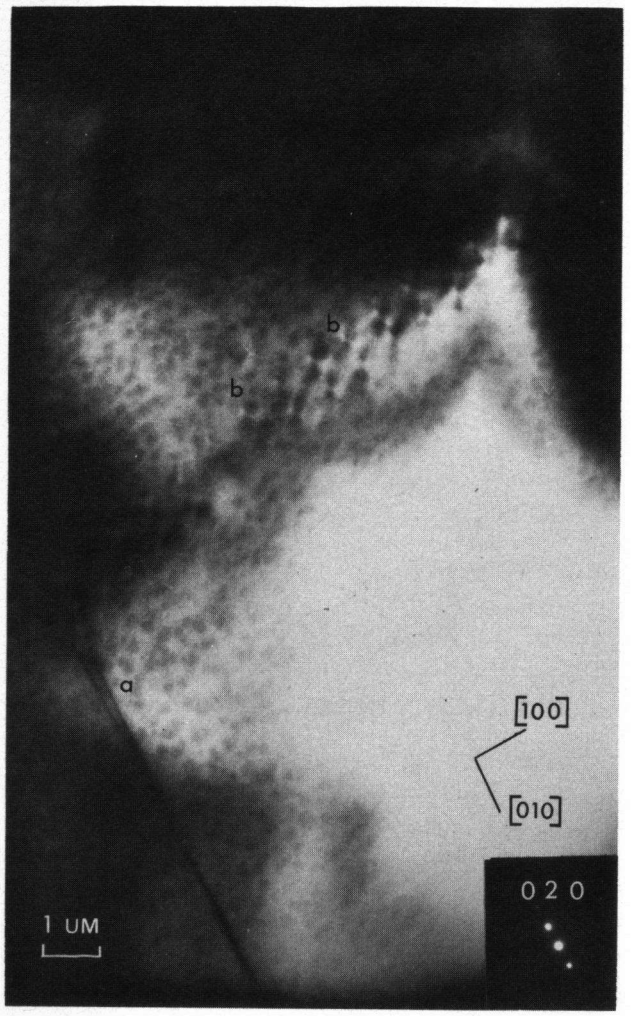

Fig. 40. Contrast analysis of Fig. 39 for $\mathbf{g} = 020$. Both dislocation types, $\mathbf{b} = [100]$ and $\mathbf{b} = [001]$, should be out of contrast ($\mathbf{g} \times \mathbf{b} = 0$); low residual contrasts are still present because the condition $\mathbf{g} \times \mathbf{b} \wedge \mathbf{u} = 0$ is not satisfied, especially in (a) where $\mathbf{u}$ is almost parallel to $\mathbf{g}$.

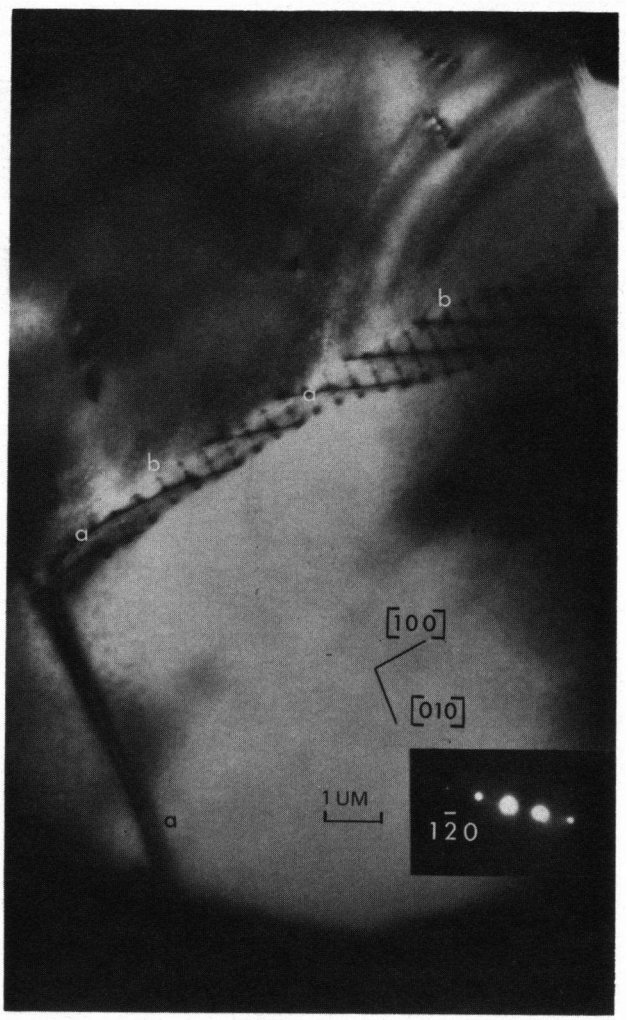

Fig. 41. Contrast analysis of Fig. 39 for $\mathbf{g} = 1\bar{2}0$. The dislocations $\mathbf{b} = [100]$ (a) are in contrast ($\mathbf{g} \times \mathbf{b} \neq 0$); the dislocations $\mathbf{b} = [001]$ (b) have residual contrast because $\mathbf{g} \times \mathbf{b} \wedge \mathbf{u} \neq 0$.

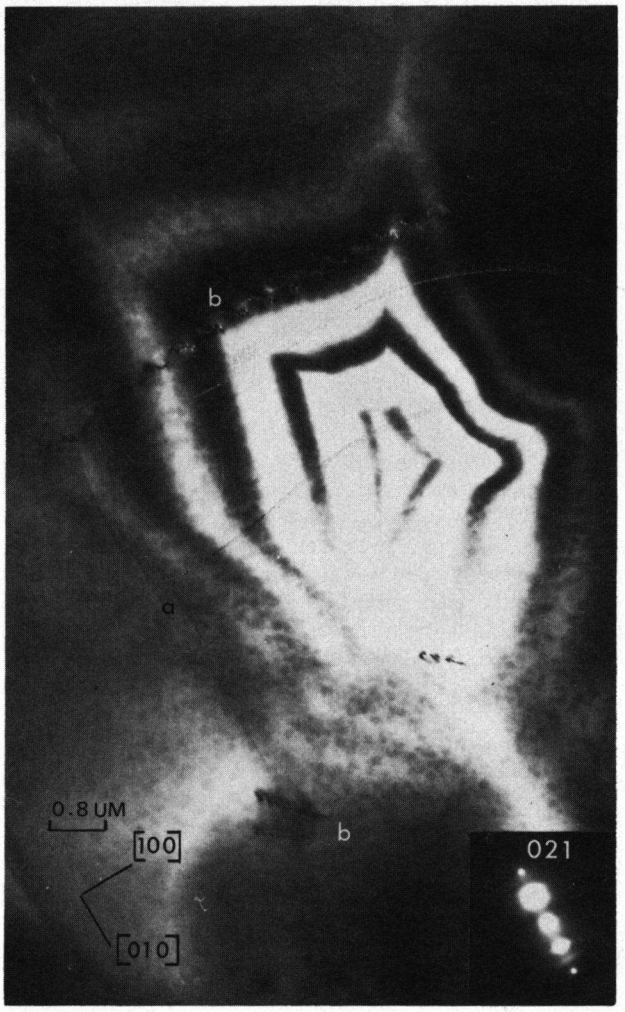

Fig. 42. Contrast analysis of Fig. 39 for $\mathbf{g} = 021$. The $\mathbf{b} = [001]$ dislocations are in contrast, while the $\mathbf{b} = [100]$ dislocations are almost out of contrast.

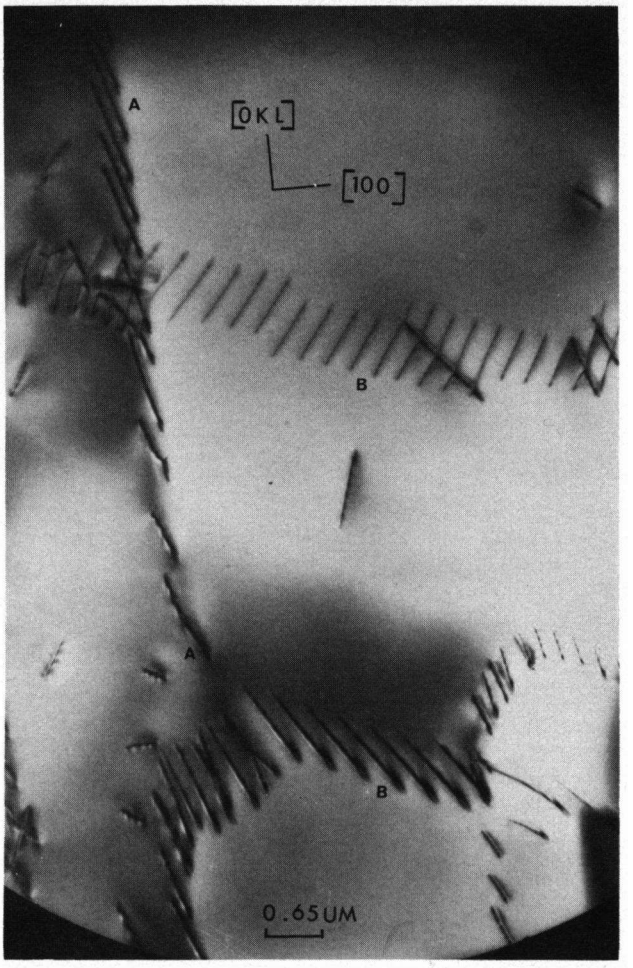

Fig. 43. In the matrix more equidimensional subgrains of dislocations are present, bounded by tilt boundaries (A) along (100) and cross arrays (B); all dislocations have $\mathbf{b} = [100]$.

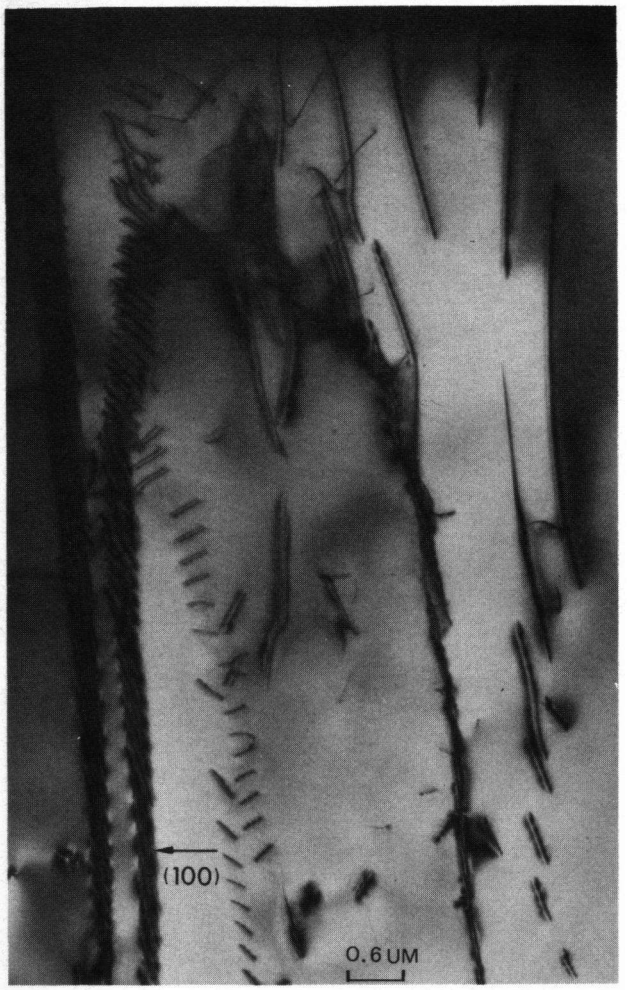

Fig. 44. Tilt boundaries along (100), constantly formed and broken up in a climb controlled process, forming a dynamically stable situation in the matrix.

DEVELOPMENT OF THE DISLOCATION ARRANGEMENT AND THE DEFORMATION PROCESS

The porphyroclasts (Table 4)

The subgrain structure indicates that, by analogy with metals deformation, the (100) tilt boundaries are produced by high temperature creep. The subgrains are either in sheet form parallel to (100), or as elongate cells parallel to [010] (see Green & Radcliffe, 1972a, b). The poorly developed (001) subboundaries, defining these elongate structures, are composed of screw dislocations, and in general have a higher energy than the edge dislocation arrays (Cottrell, 1953). The origin of these screw dislocations is uncertain, but they are likely to be either remnants of an earlier dislocation arrangement (earlier deformation event), or form a part of the glide-climb processes operative in the high temperature creep. A possible process for the development of the screw dislocation arrays in (001) is considered to be climb in a pre-existing dislocation arrangement. The screw dislocations were left behind when the climb removed the edge dislocations, and were pinned to the (100) tilt boundaries (see also Green & Radcliffe, 1972a, b). The screw dislocation spacing in the (001) plane is considerably larger than the edge dislocation spacing in the (100) plane, indicating a considerable rearrangement of the screw dislocations by glide.

The {0kl} cross arrays indicate activity of dislocations in these slip plane configurations, but the dislocations have also undergone climb into low angle (and low energy) tilt boundaries.

The following features point to the influence of dynamic recovery during creep:

1. low density of cross arrays;
2. low individual or free dislocation density;
3. closely spaced (100) arrays;
4. bowing out of screw dislocations from (100) into the (001) plane.

However, static recovery as suggested by Green & Radcliffe (1972b) is most unlikely both in this material and in the Anita Bay dunite examined by Boland et al. (1971),

	PORPHYROCLASTS	MATRIX	
grain size	0.5 to 3 mm	0.03 to 0.3 mm	
subgrain size	> 10 to 50 μm	10 to 50 μm	< 5 μm
dislocation density/cm^2	$9x10^6$ to $2x10^8$	$1.5x10^8$ to $5x10^8$	10^7 to $4x10^7$
cross arrays	few	many	
twist boundaries		many	
(100) array spacings	0.6 to 6 μm regular	> 3 μm irregular	
(100) dislocation spacings	0.09 to 0.7 μm regular	0.15 to 0.5 μm irregular	
subgrain shape	flattened//(100) or slightly elongated// [010]	equidimensional	
optical character	scalloped grain boundaries	foam texture and straight boundaries and triple point junctions	not visible
kink bands (optically visible)	many//(100)		
polygonization by:	dynamic recovery	dynamic recovery/ dynamic recrystallization	dynamic recrystallization

Table 4. Differences between olivine porphyroclasts and matrix grains observed with optical and electron microscopy techniques.

as the porphyroclasts indicate that slip polygonization (Friedel, 1964, p. 250) or dynamic recovery is active. Both processes lower the overall dislocation density, and result in subgrain arrangements. The dynamic recovery process refers to polygonization during deformation which is driven by the external stresses in addition to the thermal stresses and thermal activation (Jonas et al., 1968). Rate controlling mechanisms are climb and cross slip. The slip polygonization (Friedel, 1964) suggests a process in which the 'polygonized' walls are created by slip of edge dislocations.

The difference between these two processes is difficult to prove in the porphyroclasts, but tends to be in favour of the dynamic recovery because the distance of the dislocations in the (100) arrays has a constant value, pointing to a climb-controlled process. The structures in the mylonite resemble those found in metallic and ceramic systems undergoing dynamic recovery (Jonas et al., 1968; Mc.Queen, 1968a, b; Mc.Queen & Hockett, 1970). It can be concluded that the dynamic recovery was operative in this material, resulting in a dynamically stable but not static dislocation substructure.

The petrofabric studies show that the porphyroclasts have a γ_{ol} fabric, and have experienced a strain history different from the matrix material, although the matrix is obviously derived from the porphyroclasts. At least in the samples examined, most of the recrystallization of the porphyroclasts occurs at the grain boundaries where large inhomogeneous strains are evident.

The absence of strain-free nuclei in the porphyroclasts suggests that the recrystallization process occurs by a polygonization process rather than by the more classical nucleation and grain growth processes suggested to operate in the matrix.

The matrix (Table 4)

The matrix is obviously accommodating most of the strain in the rock. The deformation process appears to be cyclical both in time and in space in that certain regions have undergone severe deformation without recrystallization (large subgrains 10 to 50 um with free dislocations), while other regions have commenced recrystallization (subgrains smaller than 5 um, with very few dislocations in the subgrains). This situation changes as the deformation continues.

The effect of dynamic recovery is not as evident in the matrix material, as shown by the following features:

1. the (100) arrays are more widely spaced;
2. the dislocations in the (100) arrays are irregularly arranged with larger spacings;
3. the free dislocation density is high;
4. there are significantly more cross arrays;
5. fewer screw dislocations are associated with the formation of cell walls.

In the matrix, a process of dynamic recrystallization proceeds concurrently with the deformation after a critical strain was surpassed (see also description for metals deformation: Mc.Queen, 1968a, b; Mc.Queen & Bergerson, 1972).

Nuclei result from the formation of high-angle boundaries by the accumulation of dislocations in the subboundaries (e.g. along pre-existing (100) tilt boundaries). As these nuclei grow, they are deformed and develop a dislocation arrangement that gives rise to another wave of nucleation. In this cyclical process the dynamic recovery is still present, giving rise to some analogy with the dislocation substructure in the porphyroclasts.

To a first approximation it may be assumed that both porphyroclasts and matrix experienced the same temperature and stress. The strain rate and strain path in each type of grain must be the factor determining the type of dislocation substructure.

The results of experimental deformation of olivine (Phakey et al., 1972; Green & Radiclffe, 1972; Boland & Hobbs, in prep.; Boland & Paterson, in prep.) indicate that at temperatures up to 1200°C, and strain rates as low as 10^{-8} sec^{-1}, (100) [001], (110) [001] and (010) [001] slip systems are operative. The last two systems are very active. These slip systems are recorded in the material by dense bands of $\mathbf{b} = [001]$ dislocations in the larger subgrains.

The matrix also has the more typical α_{ol} fabric type. Thus the resolved stresses acting on the slip systems would be different from the values from the porphyroclasts.

The deformation process revealed by HVEM is the last significant dynamic metamorphism, involving the change from large grained porphyroclasts to the finer grained matrix grains.

If the term syntectonic or dynamic recrystallization is used, it must be concluded from our observations that such a 'mechanism' is in fact a series of dislocation-controlled mechanisms, and not a mysterious new process as sometimes implied in studies carried out before the advent of electron microscopy investigations.

Since the rock under examination is a mylonite, it is obvious that the mylonitization process in this rock is a solid state deformation with no evidence of cataclastic or brittle processes operating (Boland & Hobbs, 1973); evidence of superplasticity, as suggested to be present in some mylonites (Boullier & Gueguen, 1975), was not found.

The transition from the γ_{ol} fabric of the porphyroclasts to the α_{ol} fabric of the matrix involves both glide and polygonization processes, but the strain rates are evidently different in the two types of fabric.

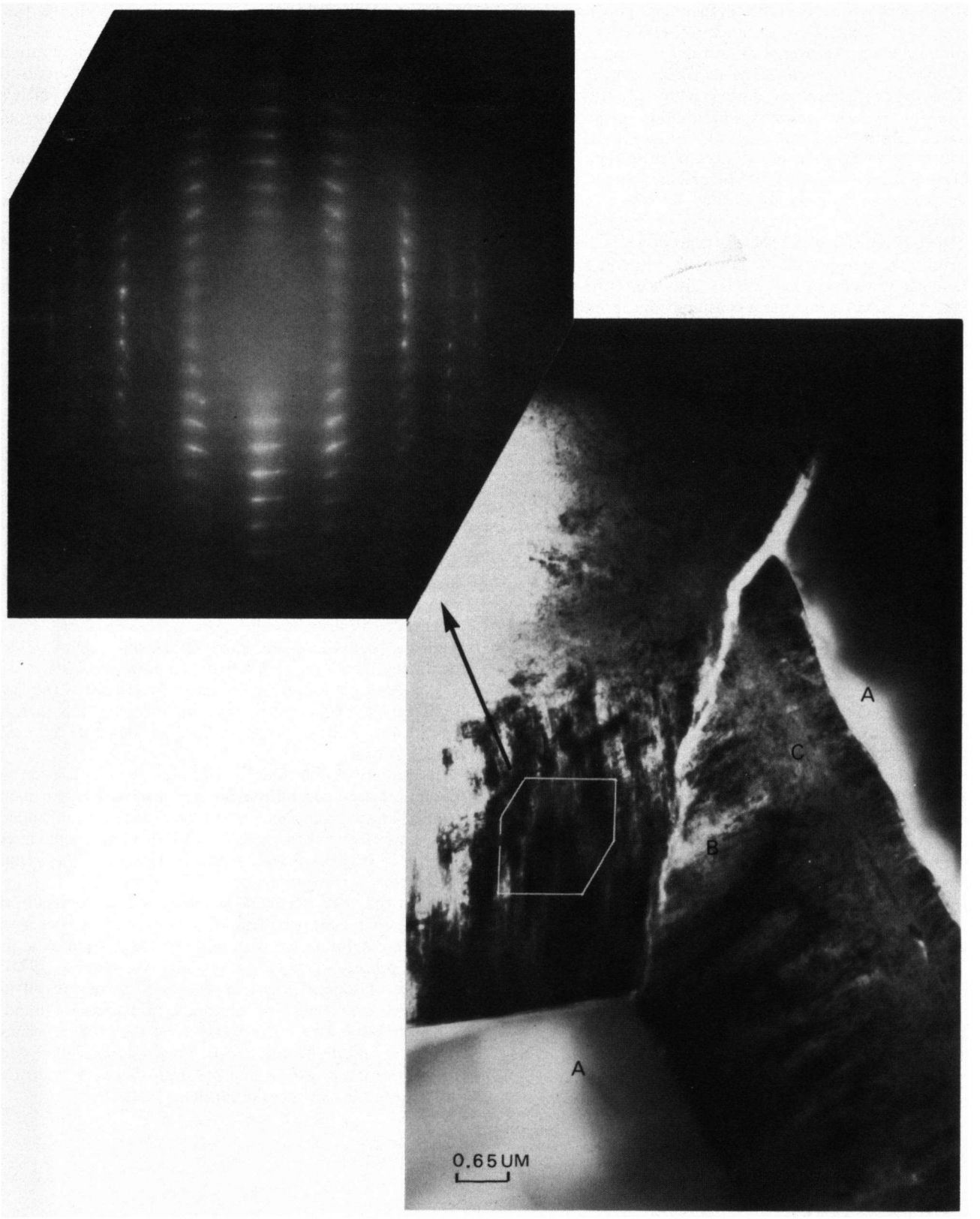

Fig. 45. Triple point junction of olivine grains (A) in the matrix. The boundary between the grains is filled with serpentine in which different structures are visible (B, C). The distorted diffraction pattern of the serpentine shows clearly the fibrous character of the material.

ACKNOWLEDGEMENTS

Under supervision of Professor E. den Tex, a research project in the Department of Petrology, Mineralogy and Crystallography of the Geological Institute, University of Leiden, already resulted in several detailed investigations in olivine bearing rocks (Collée, 1962; Avé Lallemant, 1967; Möckel, 1969). The knowledge and the experience of these investigations were indispensable for this research.

The author is greatly indebted to Professor E. den Tex for proposing the subject for this investigation, and for allowing me much freedom to pursue various aspects of it. His vast knowledge of petrofabrics, and his critical reading of the manuscript were a great support.

I am especially thankful to Dr. J. N. Boland for introducing me into the electron microscopy in Oxford, and the fruitful co-operation resulted from that period. The numerous discussions on paper contributed greatly to the ultimate result.

The author wishes also to express his gratitude to Professor Sir Peter Hirsch for allowing me to use the HVEM in the Department of Metallurgy and Science of Materials, Oxford, England, and to all the staff and technicians of the laboratory, especially R. H. Donaghay.

Professor P. Hartman gave valuable comments on crystallographic problems.

Special appreciation must be expressed to Dr. G. S. Lister for his exhaustive 'Australian-type' discussions on materials science, to Drs. T. J. Calon for his valuable co-operation, and to Dr. J. P. Engels who introduced me into the petrofabric analysis techniques.

Without the co-operation of the entire staff of the Geological Institute, this study would not have been possible. I want to thank especially Mr. F. Schild; Messrs. M. Deyn, H. C. de Graaff and C. J. van Leeuwen for the preparation of the thin sections; Messrs. W. C. Laurijssen and W. A. M. Devilée for the excellent photographical work, and Mr. J. Bult together with Messrs. M. L. Brittijn, K. A. Hakkert and B. G. Henning for the preparation of the drawings.

A grant from the Molengraaff Fonds and the Netherlands Organization for the Advancement of Pure Research (ZWO) are gratefully acknowledged.

REFERENCES

Ardell, A. J., Christie, J. M. & Tullis, J. A., 1973. Dislocation substructures in deformed quartz rocks. Crystal Lattice Defects, 4, pp. 275–285.

Avé Lallemant, H. G., 1967. Structural and petrofabric analysis of an Alpine-type peridotite: the lherzolite of the French Pyrenees. Leidse Geol. Med., 42, pp. 1–57.

– & Carter, N. L., 1970. Syntectonic recrystallization of olivine and modes of flow in the upper mantle. Geol. Soc. Am. Bull., 81, pp. 2203–2220.

Barber, D. J., 1970. Thin foils of non-metals made for electron microscopy by sputter etching. Jour. Mater. Sci., 5, pp. 1–8.

Bell, T. H. & Etheridge, M. A., 1973. Microstructure of mylonites and their descriptive terminology. Lithos, 6, pp. 337–348.

Boland, J. N., 1974. Dislocation substructures in naturally and experimentally deformed olivine. In: High Voltage Electron Microscopy. Ed. P. R. Swan. Academic Press, London, pp. 312–316.

–, 1976. An electron microscope study of dislocation image contrast in olivine (Mg, Fe)$_2$SiO$_4$. Phys. Stat. Sol.,34, pp. 361–367.

– & Buiskool Toxopeus, J. M. A., 1974. High voltage electron microscopy studies of the deformation mechanisms in olivine (Mg, Fe)$_2$SiO$_4$. Eighth Internat. Cong. on Elect. Mic., Canberra, 1, pp. 478–479.

– & Hobbs, B. E., 1973. Microfracturing processes in experimentally deformed periodtite. Int. Jour. Rock Mech. Sci. and Geomech. Abstr., 10, pp. 623–626.

–, Mc.Laren, A. C. & Hobbs, B. E., 1971. Dislocations associated with optical features in naturally deformed olivine. Contr. Min. Petr., 30, pp. 53–63.

Boullier, A. M. & Gueguen, Y., 1975. S. P. mylonites, origin of some mylonites by superplastic flow. Contr. Min. Petr., 50, pp. 93–104.

Buiskool Toxopeus, J. M. A. & Boland, J. N., 1976. Several types of natural deformation in olivine, an electron microscope study. Tectonophysics, 32, pp. 209–233.

Calnan, E. A. & Clews, C. J. B., 1950. Deformation textures in face centred cubic metals. Phil. Mag., (7) 41, pp. 1085–1100.

–, 1951a. The development of deformation textures in metals – Part II. Phil. Mag., (7) 41, pp. 616–635.

–, 1951b. The development of deformation textures in metals – Part III. Phil. Mag., (7) 41, pp. 919–931.

Carter, N. L., 1971. Static deformation of silica and silicates. Jour. Geophys. Res., 76, pp. 5514–5540.

– & Avé Lallemant, H. G., 1970. High temperature flow of dunite and peridotite. Geol. Soc. Am. Bull., 81, pp. 2181–2202.

–, Baker, D. W. & George, R. P., 1972. Seismic anisotropy, flow and constitution of the upper mantle. Geophys. Mon., 16, pp. 167–190.

–, Raleigh, C. B. & Decarli, P. S., 1968. Deformation of olivine in stony meteorites. Jour. Geophys. Res., 73, pp. 5439–5461.

Collée, A. L. G., 1962. A fabric study of lherzolites with special reference to ultrabasic nodular inclusions in the lavas of Auvergne (France). Leidse Geol. Med., 28, pp. 1–102.

Cottrell, A. H., 1953. Dislocations and plastic flow in crystals. Univ. Press, Oxford, 223 pp.

Dal Vesco, E., 1953. Genesi e metamorfosi delle rocce basiche e ultrabasiche nell'ambiente mesozonale dell'orogene pennidico. Schweiz. Min. Petr. Mitt., 33, pp. 173–480.

Deer, W. A., Howie, R. A. & Zussman, J., 1962. Rockforming minerals, 1: ortho and ring silicates. Longmans, London, 333 pp.

Emmons, R. C., 1943. The universal stage (with five axes of rotation). Mem. Geol. Soc. Am., 8, 205 pp.

Etchecopar, A., 1974. Simulation par ordinateur de la déformation progressive d'un agrégat polycrystallin. Thesis Univ. of Nantes, France, 135 pp.

Friedel, J., 1964. Dislocations. Pergamon Press, Oxford, 491 pp.

Gillespie, P., Mc. Laren, A. C. & Boland, J. N., 1971. Operating characteristics of an ion-bombardment apparatus for thinning non-metals for transmission electron microscopy. Jour. Mater. Sci., 6, pp. 87–89.

Gleiter, H. & Chalmers, B., 1972. High angle grain boundaries. In: Progress in materials science, Vol. 16. Eds. B. Chalmers, J. W. Christian & T. B. Massalski. Pergamon Press, Oxford, 272 pp.

Green, H. W., 1974. Comments on paper by A. Olsen and T. Birkeland: "Electron microscope study of peridotite xenoliths in kimberlites". Contr. Min. Petr., 46, pp. 69–72.

– & Radcliffe, S. V., 1972a. Dislocation mechanisms in olivines and flow in the upper mantle. Earth Planet. Sci. Lett., 15, pp. 239–247.

–, 1972b. Deformation processes in the upper mantle. Geophys. Mon., 16, pp. 139–156.

–, 1972c. The nature of deformation lamellae in silicates. Geol. Soc. Am. Bull., 83, pp. 847–852.

Grubenmann, U., 1908. Der granat-olivinfels des Gordunotales und seine Begleitgesteine. Vjschr. Naturf. Ges. Zürich, 53, pp. 129–156.

Head, A. K., Humble, P., Clarebrough, L. M., Morton, A. J. & Forwood, C. T., 1973. Computed electron micrographs and defects identification. North Holland Publ. Comp., Amsterdam, 400 pp.

Hirsch, P. B., Howie, A., Nicholson, R. B., Pashley, D. W. & Whelan, M. J., 1965. Electron microscopy of thin crystals. Butterworths, London, 549 pp.

Honeycombe, R. W. K., 1968. The plastic deformation of metals. Edward Arnold, London, 477 pp.

Hull, D., 1965. Introduction to dislocations. Pergamon Press, Oxford, 259 pp.

Jonas, J. J., Mc. Queen, H. J. & Wong, W. A., 1968. Dynamic recovery during the extrusion of aluminium. Iron Steel Inst. London Spec. Rept., 108, pp. 49–59.

Kazakov, A. N., 1965. Microstructural orientation of olivine in rocks of the supposed upper earth mantle. Zap. Vsesoyuzn. Min. Obshch., 2nd Ser., 94, pp. 576–580 (in Russian).

Klosterman, M. J. & Buseck, P. R., 1973. Structural analysis of olivine in pallasitic meteorites: deformation in planetary interiors. Jour. Geophys. Res., 78, pp. 7581–7588.

Littlejohn, A. L. & Greenwood, H. J., 1974. Lherzolite nodules in basalts from British Columbia, Canada. Can. Jour. Earth Sci., pp. 1288–1308.

Mc.Queen, H. J., 1968a. Hot working and recrystallization of facecentred cubic metals. Trans. Jap. Inst. Metals, 9, pp. 170–177.

–, 1968b. Deformation mechanisms in hot working. Jour. Metals, April, pp. 31–38.

– & Bergerson, S., 1972. Dynamic recrystallization of copper during hot torsion. Metal. Sci. Journ., 6, pp. 25–29.

– & Hockett, J. E., 1970. Microstructures of aluminium compressed at various rates and temperatures. Metal. Trans., 1, pp. 2997–3004.

Mercy, E. L. P. & O'Hara, M. J., 1965. Olivines and orthopyroxenes from garnetiferous peridotites and related rocks. Norsk Geol. Tidsskr., 45, pp. 457–461.

Mises, R. von, 1928. Mechanik der plastischen Formänderung von Kristallen. Zeitschr. angew. Math. Mech., 8, pp. 161–185.

Möckel, J. R., 1969. Structural petrology of the garnet peridotite of Alpe Arami (Ticino, Switzerland). Leidse Geol. Med., 42, pp. 61–130.

–, 1970. Description and use of some Fortran IV computer programs for petrofabric analysis. Internal Rept. Dept. Petr. Min. Cryst., Univ. Leiden, The Netherlands, 37 pp.

Nicolas, A., Bouchez, J. L. & Boudier, F., 1972. Interprétation cinématique des déformations plastiques dans le massif de lherzolite de Lanzo (Alpes piémontaises) – comparaison avec d'autres massifs. Tectonophysics, 14, pp. 143–171.

–, Boudier, F. & Boullier, A. M., 1973. Mechanisms of flow in naturally and experimentally deformed peridotites. Am. Jour Sci., 273, pp. 853–876.

O'Hara, M. J. & Mercy, E. L. P., 1963. Petrology and petrogenesis of some garnetiferous peridotites. Trans. Roy. Soc. Edinburgh, 65, pp. 251–314.

–, 1966. Garnet peridotite and eclogite from Bellinzona, Switzerland. Earth Planet. Sci. Lett., 1, pp. 295–300.

Paterson, M. S., 1969. The ductility of rocks. In: Physics of strength and plasticity. Ed. A. S. Argon. The M. I. T. Press, London, pp. 377–392.

– & Weiss, L. E., 1961. Symmetry concepts in the structural analysis of deformed rocks. Geol. Soc. Am. Bull., 72, pp. 841–882.

Phakey, P., Dollinger, G. & Christie, J., 1972. Transmission electron microscopy of experimentally deformed olivine crystals. Geophys. Mon., 16, pp. 117–138.

Ragan, D. M., 1969. Olivine recrystallization textures. Min. Mag., 37, pp. 238–240.

Raleigh, C. B., 1968. Mechanisms of plastic deformation of olivine. Jour. Geophys. Res., 73, pp. 5391–5406.

– & Kirby, S. H., 1970. Creep in the upper mantle. Min. Soc. Am. Spec. Pap., 3, pp. 113–121.

Rost, F., Wannemacher, J. & Grigel, W., 1974. Die Ultramafitite der Alpe Arami und Croveggio Tessin (Schweiz). Schweiz. Min. Petr. Mitt., 54, pp. 353–369.

Stanton, R. L., 1972. Ore petrology. McGraw-Hill, New York, 713 pp.

Steeds, J. W., 1973. Introduction to anisotropic elasticity theory of dislocations. Clarendon Press, Oxford, 274 pp.

Taylor, G. I., 1938. Plastic strain in metals. Jour. Inst. Metals, 62, pp. 307–324.

White, S., 1975. The effects of polyphase deformation on the intracrystalline defect structures of quartz, part II. N. Jahrb. Min. Abh., 123, pp. 237–252.

Yoshino, G., 1961. Structural petrological studies of peridotite and associated rocks of the Higashi-akaishi-yama District, Shikoku, Japan. Jour. Sci. Hiroshima Univ., C, 3, pp. 343–402.

–, 1964. Ultrabasic mass in the Higashi-akaishi-yama District, Shikoku, Southwest Japan. Jour. Sci. Hiroshima Univ., C, 4, pp. 333–364.

Young, C., 1969. Dislocations in the deformation of olivine. Am. Jour. Sci., 267, pp. 841–852.